THE ASTRONOMICAL JOURNAL VOLUME 87, NUMBER 7 JULY 1982

THE DYNAMICS OF RICH CLUSTERS OF GALAXIES. I. THE COMA CLUSTER

S. M. KENT
Harvard-Smithsonian Center for Astrophysics, 60 Garden Street, Cambridge, Massachusetts 02138

J. E. GUNN
Peyton Hall, Princeton University, Princeton, New Jersey 08540
Received 16 February 1982

ABSTRACT

The structure and dynamics of the Coma cluster are analyzed using self-consistent equilibrium dynamical models. Observational material for Coma is culled from a variety of sources. Projected surface, density, and velocity-dispersion profiles are derived extending out to a radius of 3° from the cluster center, which are essentially free from field contamination. Segregation of galaxies by luminosity and morphology are discussed and a quantitative estimate of the latter is made. The method of constructing self-consistent dynamical models is discussed. Four different forms of the distribution function are analyzed allowing for different possible dependences of f on energy and angular momentum. Properties of typical models that might resemble actual clusters are presented, and the importance of having velocity-dispersion information is emphasized. The effect of a central massive object such as a cD galaxy on the core structure is illustrated. A comparison of these models with Coma reveals that only models with a distribution function in which the ratio of tangential to radial velocity dispersions is everywhere constant give acceptable fits. In particular, it is possible to rule out models that have isotropic motions in the core and predominantly radial motions in the halo. For $H_0 = 50$, the best-fitting models give a total projected mass inside 3° of $2.9 \times 10^{15}\ M_\odot$, a core radius of 340–400 kpc (8.5′–10′), an upper limit to any central massive object of $\sim 10^{13}\ M_\odot$, and a mass-to-blue-light ratio of $M/L = 181$. From cosmological considerations the cluster "edge" is determined to lie at $r \sim 5°$–6°. The possible distribution of "dark matter" in Coma is discussed and it is argued that this distribution cannot be significantly different from that of the galaxies. The dynamics of morphological segregation are examined quantitatively, and are explained at least qualitatively. Finally, it is shown that x-ray maps of the distribution of an intracluster medium cannot place strong constraints on the core structure of a cluster without having simultaneous information on the temperature distribution.

I. INTRODUCTION

Clusters of galaxies are the largest dynamically bound entities in the universe. A major advantage to studying the dynamics of clusters is that one can measure not only the spatial distribution but also the radial velocities of the constituent galaxies, measurements that are difficult to make for other dynamical systems such as globular clusters and individual galaxies. The chief drawback with clusters of galaxies is the irregular appearance of most, making any interpretation of their dynamics difficult. However, the richest clusters possess a regularity and smoothness which suggest that they have attained a state of dynamical equilibrium, and it is on these systems that we focus our attention.

In the standard idealized picture of cluster formation (Gunn and Gott 1972), clusters originate in the early universe as small perturbations on an otherwise uniform background density. These perturbations eventually grow and collapse out of the expanding Hubble flow. Galaxies may form either before or during the collapse phase. After undergoing a period of violent relaxation, the cluster proper settles down to a state of dynamical equilibrium. Material outside the initial perturbation continues to dribble onto the cluster long after the initial collapse is complete.

Various n-body calculations have been made to simulate this collapse scenario, and they produce results that, at least qualitatively, resemble real clusters (Peebles 1970; White 1976). However, these simultations are not well suited to studying the detailed structure and dynamics of clusters, and for this reason we have chosen to use self-consistent analytical dynamical models to study the endpoint of cluster formation. As a point of focus, in this paper we concentrate on the Coma cluster, for which a vast amount of published data already exists.

Different aspects of the structure and dynamics of Coma have been explored by numerous past investigators (e.g., Zwicky 1957; Rood 1975, Rood *et al.* 1972, hereafter referred to as RPKK; Bahcall 1973; Gregory 1975a; Gregory and Tifft 1976; Tifft and Gregory 1976; Abell 1977). Yet certain basic questions remain unanswered; e.g., are the galaxy orbits in Coma primarily isotropic or radial? The only investigation to self-consistently match both surface-density and velocity-dispersion profiles with a single dynamical model has been the work of RPKK, who found a fair match with an isotropic King (1966) model. Since that work, the number of available redshifts has increased threefold, and it is now possible to reconsider the dynamics of Coma in greater detail.

We will pay particular attention to the following points:

(1) The effects of anisotropy in the velocity dispersion and variations in the energy-distribution function on the cluster structure;

(2) The effect on the core structure of a massive central object;

(3) The dynamical consequences of morphological segregation;

(4) Cosmological infall and the edge of a cluster;

(5) The distribution of "dark matter" in a cluster;

(6) The implications of x-ray observations for the distribution of gravitating material in a cluster.

The necessary radial velocity data are collected together in Sec. II. New and repeated redshifts are reported for a number of galaxies in the central regions of the cluster. Cluster membership is determined and a velocity-dispersion profile is derived. In Sec. III, a composite surface-density profile is derived using both galaxy surveys published in the literature and the radial velocity data of Sec. II. In Sec. IV, the segregation of galaxies by magnitude and morphology is investigated. In Sec. V, the method of constructing dynamical models is presented, and four different forms for the distribution function are introduced. In Sec. VI, the properties of these models are discussed and examples are given illustrating the characteristic features of each type of distribution function as reflected observationally. Amazing examples are shown of models with virtually identical surface-density profiles but otherwise completely different internal dynamics. In Sec. VII, a detailed comparison is made with the Coma cluster. It will be shown that only one class of models (which includes the isotropic King models) is consistent with the observed density and velocity-dispersion profiles for Coma. Based on these models, additional topics are taken up in Sec. VIII, including cosmological infall, morphological segregation, and x-ray emission from an intracluster medium. Our conclusions are summarized in Sec. IX.

II. RADIAL VELOCITIES

Because the Coma cluster has been so widely studied over the years, virtually all the needed observations are available in the literature.

a) Radial Velocities

From an extensive survey of the literature we have compiled a list of redshifts for galaxies in the Coma cluster and its surrounding environs out to a radius of 6° from the center. For reference we present the entire list in Table I. Most of the columns are self-explanatory. A variety of designations have been assigned by different investigators and are usually explained in the individual references. Column (6) gives the distance of a galaxy from the cluster center (taken to be NGC 4874) in arcmin. Column (7) gives m_p magnitudes, either as listed by Zwicky and Herzog (1963, 1966) or converted to that system. Column (8) gives the morphological type ($1 = \mathrm{E}$, $3 = \mathrm{S0}$, $5 = \mathrm{Sp}$, $7 = \mathrm{Irr}$, other numbers are intermediate types). Galactocentric velocities are listed in column (9). We have attempted to list the original source for most of the redshifts, although many are repeated in later compilations (in some cases with slightly different values). One of us (J.E.G.) has obtained redshifts for a number of fainter galaxies in and around the cluster core using the Hale 5-m telescope, and such entries in Table I are so marked. When multiple measurements have been made, all are listed; in the subsequent analysis a straight average is taken. Morphological types are normally taken from the same source as the redshift, but a few are taken from Tifft (1979).

Contained within Table I are two complete samples first compiled by Tifft and Gregory (1976) from the *Catalog of Galaxies and Clusters of Galaxies* (Zwicky and Herzog 1963, 1966). One sample is complete to $m_p \leqslant 15.7$ within a radius of 3° from the cluster center, and the other is complete to $m_p < 15.0$ within a radius of 6°. We will find these two samples to be extremely useful in delineating the cluster structure at large distances from the center.

b) Cluster Membership

A plot of all galaxies from Table I with measured velocities as a function of radius is shown in Fig. 1. As explained below, we have adopted the position of NGC 4874 ($\alpha = 12^{\mathrm{h}}57^{\mathrm{m}}18$, $\delta = 28°13'8$) as the cluster center. Two lines are drawn in Fig. 1 which we have used to separate cluster members from foreground and background galaxies. As previous investigators have noted (e.g., Tifft and Gregory 1976), Coma and its environs are well isolated in redshift space; there is no uniform "field" to contend with. This fact is again evident in Fig. 1 where, with few exceptions, there is little uncertainty as to cluster membership out to a radius of at least 3° or 4°. The Coma cluster resides within a much larger surrounding unbound supercluster (Gregory and Thompson 1978) consisting of isolated galaxies and groups. Although the mean density within the supercluster is much lower than for the Coma cluster proper, it can be a significant source of contamination at large radii. Following Tifft and Gregory (1976), we restrict our analysis to the region $R < 3°$. Below we shall estimate the magnitude of any contamination and consider more carefully the question of an "edge" to the cluster.

c) Velocity-Dispersion Profile

In Table II, we list the velocity-dispersion profile de-

TABLE I. Radial velocities of galaxies in Coma within $R = 6°$.

NGC/IC	Zw	Other	Ra (1950)	Dec (1950)	R (')	Mag	Morph	Vo	Ref
(1)	(2)	(3)	(4)	(5)	(6)	(7)	(8)	(9)	(10)
	159-19		12 32.9	29 47.	331.8	14.9	5	4752	TG76
								4653	CR3
N4562	129-8		12 33.0	26 08.	346.3	14.6	5	1379	TG76
								1301	CR3
N4555	159-21		12 33.2	26 48.	330.3	13.5		6685	CR2
N4556W	159-22A		12 33.3	27 12.	323.0	14.4		7980	CR2
N4556E	159-22B		12 33.3	27 12.	323.0	.		7395	CR2
N4559	159-24		12 33.4	28 14.	314.2	10.7	5	802	RC2
N4565	129-10		12 33.8	26 15.	333.6	10.3	5	1122	RC2
I3585	159-28		12 34.1	27 07.	313.8	15.0		7403	CR2
I3600	159-35	CT19	12 35.1	27 24.	297.1	15.5	1	4591	TG73
I3599	159-34	CT20	12 35.1	26 59.	302.9	15.7	3	6432	TG73
N4585	159-37		12 35.7	29 13.	288.7	14.6		7411	TG76
	159-42	CT8	12 36.7	28 01.	271.2	15.4	1	8036	TG73
I3618	159-41	CT18	12 36.7	26 57.	282.9	15.5	1	6509	TG73
I3620	159-44	CT6	12 36.8	28 11.	269.4	15.6	5	6547	TG73
	159-43	CT7	12 36.8	28 03.	269.8	15.3	1	6694	TG73
I3623	159-46	CT17	12 36.9	27 23.	273.8	15.2	1	6960	TG73
I3645	159-49	CT16	12 38.0	26 48.	269.2	15.4	3	6532	TG73
I3651	159-50	CT15	12 38.3	27 00.	261.6	14.4	3	4777	TG73
	159-51A	CT5	12 38.4	28 15.	248.2	15.4	3	9489	TG73
	159-51B		12 38.4	28 15.	248.2	.		7883	RC2
	159-52		12 38.4	29 45.	262.7	14.9		9377	TG76
	159-54	CT14	12 38.7	27 01.	256.2	15.5	3	4477	TG73
	159-55	CT4	12 38.8	28 08.	243.1	15.6	3	7631	TG73
N4614	129-15		12 39.0	26 18.	268.6	14.2	5	4917	TG76
								4778	CR3
N4615	129-18		12 39.1	26 20.	266.5	13.8	5	4795	TG76
								4677	CR3
N4627	188-15		12 39.5	32 51.	359.1	13.3	1	745	CR3
N4631	188-16		12 39.7	32 49.	355.9	9.8	5	638	RC2
	159-57	CT11	12 40.2	27 24.	230.7	15.6	1	6522	TG73
	159-58	CT13	12 40.3	26 55.	237.9	15.5	1	6797	TG73
	159-59	CT3	12 40.6	28 00.	219.8	14.5	3	7456	TG73
	159-61		12 40.8	31 22.	284.4	14.8		7113	TG76
	159-63	CT12	12 41.3	27 08.	221.0	15.7	1	7546	TG73
N4656	159-65		12 41.6	32 27.	323.7	10.6	5	662	RC2
	159-67	CT1	12 42.1	28 45.	201.2	14.7	3	993	TG73
	159-68	CT2	12 42.1	28 10.	199.4	15.7	5	6374	TG73
I813 E	129-22A		12 42.7	23 19.	353.7	14.4		7049	TG76
N4670	159-69		12 42.8	27 24.	197.2	12.6		1216	LMNS
								1180	K
								1112	CR1
N4673	159-70		12 43.1	27 20.	194.4	13.7	1	6997	LMNS
N4676N	159-72A		12 43.74	31 00.4	241.8	14.1	3	6631	RC2
N4676S	159-72B		12 43.76	30 59.9	241.3	.	3	6590	RC2

NGC/IC	Zw	Other	Ra (1950)	Dec (1950)	R (')	Mag	Morph	Vo	Ref
(1)	(2)	(3)	(4)	(5)	(6)	(7)	(8)	(9)	(10)
I818	159-73		12 44.2	30 00.	200.5	15.1	3	4661	K
	159-74	A1	12 44.4	26 50.	189.5	15.0	3	885	LMNS
								862	CR1
	159-75		12 44.9	27 44.	165.4	15.2		6539	GR2
I821	159-76		12 45.0	30 04.	193.9	14.5	5	6862	K
	159-77	A2	12 45.1	27 16.	170.5	14.7	3	7124	LMNS
N4692	159-78		12 45.4	27 30.	162.2	14.0	1	7917	LMNS
	159-79	A3	12 45.9	27 08.	163.6	15.2	3	6923	LMNS
	159-80		12 46.2	26 42.	172.6	15.7		7094	GR2
N4712	129-25		12 47.1	25 44.	201.5	13.5	5	4536	CR2
	159-82		12 47.1	31 07.	217.4	14.8		8174	TG76
	159-83	A4	12 47.2	27 10.	147.1	14.9	1	7435	LMNS
N4715	159-85		12 47.4	28 05.	129.6	15.4	2	6902	K
	129-26		12 47.6	25 17.	218.4	15.4		6370	TG79
N4719	188-24		12 47.7	33 25.	334.3	14.2	5	7170	TG76
N4721	159-86		12 47.8	27 36.	129.9	15.2		7858	GR1
N4725	129-27		12 48.0	25 46.	192.1	10.2	5	1108	LMNS
								1213	CR1
N4728	159-87		12 48.0	27 43.	125.5	15.6	3	6528	LMNS
	159-89	A5	12 48.3	28 06.	117.7	14.8	1	7442	K
								7566	CR1
								7412	TG73
	159-90		12 48.5	27 39.	120.2	15.5	5	8355	GR1
N4735	159-91		12 48.6	29 12.	127.0	15.1	5	6687	CR2
								6614	TG76
N4738	159-92		12 48.7	29 04.	122.4	14.9	3	4585	K
								4801	GR1
								4791	TG76
	159-93		12 48.8	27 23.	122.2	15.3	5	5437	K
								5453	CR1
								5449	TG76
I826	159-95		12 48.8	31 19.	214.9	14.9		7153	TG76
N4745	159-94		12 48.9	27 42.	114.2	15.4	5	7160	K
								7597	GR1
N4747	129-28		12 49.3	26 02.	168.6	13.2	5	1216	CR1
	159-97		12 49.6	27 18.	115.0	15.4	7	6546	GR1
								6477	TG76
	159-98		12 49.6	27 51.	102.9	15.5		8188	GR1
	159-99		12 50.1	27 01.	119.0	15.7	5	7981	GR1
I831	159-100		12 50.2	26 45.	128.5	15.5		6364	GR1
	-	TT27	12 50.2	29 08.	106.7	.	1	58813	TT77
	159-101		12 50.3	27 40.	97.2	15.3	7	7855	CR1
								7837	GR2
	159-102	A7	12 50.4	28 39.	92.9	14.5	3	7112	K
								7010	TT75
	159-103		12 50.6	32 22.	262.4	14.8		6894	TG76

TABLE I. (continued)

NGC/IC	Zw	Other	Ra (1950)	Dec (1950)	R (')	Mag	Morph	Vo	Ref
(1)	(2)	(3)	(4)	(5)	(6)	(7)	(8)	(9)	(10)
	159-104	A8	12 50.7	27 21.	100.9	15.0	5	6154	CR1
	129-29		12 50.7	25 32.	183.6	15.5		1224	TG79
I832	159-105		12 51.4	26 43.	119.0	15.0	1	7003	CR1
	159-106		12 51.4	29 15.	97.6	15.6		7890	GR1
	159-107		12 51.4	29 51.	123.3	15.3		13861	GR1
	159-110		12 51.6	29 52.	122.5	14.8		6529	GR1
								6309	TG76
N4787	159-111		12 51.7	27 20.	90.5	15.5	4	7636	GR1
N4789B	-		12 51.7	27 26.	87.0	.		375	RC2
N4788	159-112		12 51.8	27 35.	81.2	15.4	5	6462	GR1
N4789	159-113	TT2	12 51.9	27 20.	88.3	13.3	1	8375	LMNS
								8224	TT75
	159-114		12 52.1	28 39.	71.6	15.5		7132	GR1
	159-115		12 52.2	27 12.	90.5	15.6		6203	GR1
N4793	159-116	TT20	12 52.2	29 12.	87.6	12.3	5	2544	LMNS
								2388	TT75
								2464	TG76
	159-117		12 52.3	30 48.	166.8	15.7		6348	GR2
N4798	159-118		12 52.5	27 41.	70.2	14.3	4	7679	LMNS
	159-119	ZW160-14	12 52.5	28 41.	67.4	15.7		7503	GR1
	160-15	TT29	12 53.0	28 05.	56.0	15.5	5	7443	GR1
								7498	TT77
	160-16		12 53.0	28 44.	62.8	15.7		7185	GR1
N4807A	160-17A		12 53.1	27 47.	60.3	14.4	1	6853	K
								6980	TG76
N4807B	160-17B		12 53.1	27 47.	60.3	.	3	7127	K
	160-18		12 53.1	27 56.	56.9	15.3	4	7092	GR1
I3900	160-19		12 53.3	27 31.	66.9	14.8	2	7177	LMNS
	160-20	TT30	12 53.7	27 57.	49.0	15.5	7	4887	GR2
								4982	TT77
								4832	RC2
S	160-20A		12 53.7	27 55.	49.7	.		7424	GR1
N4816	160-21		12 53.8	28 01.	46.5	14.8	1	6862	K
	160-22	CT29	12 54.0	26 38.	104.7	15.2	1	6292	TG73
	160-23		12 54.0	28 01.	44.0	15.5	1	7100	GR1
N4821	160-24		12 54.1	27 13.	73.3	15.0	3	6980	LMNS
N4819	160-25		12 54.1	27 15.	71.6	14.0	5	6702	LMNS
	160-27		12 54.1	28 06.	41.5	15.6	1	6771	GR1
	-	TT25	12 54.2	28 32.	43.3	16.0		7259	TT75
								6945	U
	-	TT28	12 54.2	27 37.	54.0	.	1	12051	TT77
N4827	160-28	TT3	12 54.3	27 26.	61.2	14.1	1	7656	LMNS
								7455	TT75
								7498	TG76
N4828	160-29		12 54.3	28 17.	38.2	15.4	3	6141	GR1
	160-30		12 54.3	30 59.	169.4	15.1		7862	GR2
	160-31		12 54.4	27 22.	63.6	15.7	5	6852	GR1
I3918	130-2		12 54.4	22 39.	336.9	15.6		6512	TG79
I835	160-32	CT30	12 54.5	26 45.	95.7	14.9	3	7747	TG73
	160-33	A9	12 54.5	27 10.	73.1	15.1	1	6254	K
								6310	CR1
	160-34		12 54.5	29 12.	68.0	15.2		8030	GR1
	160-36	A10	12 54.5	30 59.	168.9	14.7	5	7286	K
	-	TT31	12 54.5	26 49.	92.0	.	1	36624	TT77
	189-2		12 54.5	32 43.	271.4	15.1		13458	RC2
	160-35		12 54.6	29 19.	73.5	15.4		7528	GR1
	160-37		12 54.8	27 44.	43.4	15.0	3	7341	GR1
	160-38	A11	12 54.8	29 18.	71.4	14.8	3	7472	K
N4839	160-39	TT4	12 55.0	27 46.	40.1	13.6	1	7450	LMNS
								7376	TT75
								7449	TG76
	160-40		12 55.0	27 49.	38.1	15.3	1	5523	GR1
	-	MK55	12 55.0	27 41.	43.7	.		4889	RC2
I837	160-41		12 55.1	26 46.	92.1	15.4		7041	GR1
N4840	160-42		12 55.1	27 53.	34.5	14.8	1	6199	K
								5792	CR1
								5949	GR2
	160-43		12 55.1	28 28.	30.9	15.4	4	7078	GR1
N4841W	160-44A		12 55.1	28 45.	41.5	13.5	1	6708	K
								6892	TG76
N4841E	160-44B		12 55.1	28 45.	41.5	14.2	1	6224	TG76
	160-45		12 55.2	27 07.	71.8	15.5		6514	GR1
N4842S	160-46A		12 55.2	27 45.	39.0	14.9	1	7518	LMNS
								7496	TG76
N4842N	160-46B		12 55.2	27 45.	39.0	.	3	7302	TG76
	160-47		12 55.3	28 06.	26.1	15.7	5	6163	GR1
W	160-48A		12 55.3	28 09.	25.3	15.3	3	6044	GR1
								6082	RC2
E	160-48B		12 55.3	28 09.	25.3	16.1	3	6948	GR1
N	160-49A		12 55.4	28 27.	27.0	15.5	3	7359	GR2
	160-50		12 55.4	29 55.	103.9	15.2		5319	GR1
	-	TT5	12 55.5	28 20.	23.0	16.0	2	8151	TT75
								8175	U
	160-51		12 55.6	27 08.	69.1	15.2	4	7371	GR1
	160-52		12 55.6	27 11.	66.2	15.5	3	7979	GR1
	160-53		12 55.6	28 05.	22.7	15.7	2	7205	GR1
N4848	160-55	TT6	12 55.7	28 31.	26.0	14.2	5	7224	LMNS
								7271	TT75
	-	A1255+24	12 55.7	24 37.	217.7	.		6650	RC2
N4849	160-56	CT32	12 55.8	26 40.	95.6	14.5	1	5829	LMNS
								6029	TG73
	160-57		12 55.8	28 24.	20.9	15.5	3	7414	GR1

TABLE I. (continued)

NGC/IC	Zw	Other	Ra (1950)	Dec (1950)	R (')	Mag	Morph	Vo	Ref
(1)	(2)	(3)	(4)	(5)	(6)	(7)	(8)	(9)	(10)
	160-58	TT32	12 55.8	28 59.	48.7	15.5	5	7623	GR2
								7674	TT77
	160-59		12 55.8	29 13.	61.9	15.2	2	7572	GR1
N4851S	160-61A		12 55.9	28 25.	20.3	15.2	3	7792	GR1
I839 N	160-61B		12 55.9	28 25.	20.3	15.9	3	6682	GR1
N	160-62A		12 55.9	29 24.	72.2	15.0	3	7850	GR1
	-	RB183	12 55.9	28 02.	20.6	16.9	3	5379	T72
	-	TT33	12 55.9	27 35.	42.3	.	9	7478	TT77
N4850	160-63		12 56.0	28 14.	15.6	15.3	3	5996	LMNS
	160-64	TT34	12 56.1	27 31.	45.1	15.4	5	7425	CR1
								7423	TT77
	160-65	RB241	12 56.1	28 17.	14.6	15.0	1	7254	K
								7185	TG76
	-	RB243	12 56.1	28 19.	15.2	16.5	1	5905	T72
	-	RB188	12 56.1	27 57.	22.1	16.5	1	6906	T72
	160-66		12 56.2	27 22.	53.4	15.3	3	7872	GR1
	160-67	A12	12 56.2	27 26.	49.5	15.4	6	7666	K
								7704	CR1
N4853	160-68		12 56.2	27 51.	26.2	14.2	3	7561	LMNS
I3943	160-69		12 56.2	28 23.	15.9	15.6	4	6827	GR1
								6893	G
N4854	160-70		12 56.4	27 57.	19.7	15.2	1	8062	K
								8143	G
								8276	TG76
I3946	160-A1	C1	12 56.40	28 05.0	13.6	15.3	3	6107	LMNS
								5892	G
								6009	TG76
	-	RB252	12 56.4	28 21.	12.6	16.1	3	5940	T72
I3947	160-A2		12 56.45	28 03.5	14.1	15.6	3	5703	T72
								5512	G
	-	RB209	12 56.5	28 05.	12.6	16.6	3	5521	T73
								5384	G
	-	RB214	12 56.5	28 04.	13.3	16.7	3	7008	T73
								6975	TT75
								6749	G
								6865	U
	-	RB257	12 56.5	28 14.	9.0	16.3	3	5676	T72
I3949	160-A3		12 56.53	28 06.4	11.3	14.9	3	7538	LMNS
								7450	G
								7419	TG76
N4859	160-71		12 56.6	27 05.	69.2	14.8	5	7037	K
	-	RB260	12 56.6	28 14.	7.7	16.7	3	8320	T72
N4858	160-A4	TT9	12 56.63	28 23.2	11.9	15.5	5	9398	LMNS
								9491	TT75
	160-A5		12 56.63	28 29.8	17.6	15.3	3	8028	TG76
N4860	160-A6	TT24	12 56.67	28 23.7	12.0	14.7	1	7877	LMNS
								7905	TT75
I3955	160-A7		12 56.68	28 16.0	7.0	15.6	3	7868	T72
								7616	G
								7687	TG76
	-	RB262	12 56.7	28 11.	6.9	16.2	3	6451	T72
	160-73	A13,TT8	12 56.7	27 55.	19.8	15.1	5	5366	K
								5354	TT75
								5414	G
								5388	RC2
I3957	160-A8		12 56.70	28 02.4	13.0	15.6	1	6317	T73
	-	RB261	12 56.7	28 14.	6.3	16.9		6905	T72
I3959	160-A9		12 56.72	28 03.4	12.0	15.2	1	7094	T73
								6955	G
								7006	TG76
I3960	160-A10		12 56.72	28 07.6	8.7	15.5	3	6682	T72
	-	RB223	12 56.8	28 08.	7.7	17.2	1	6880	LMNS
I3963	160-A11		12 56.80	28 02.8	12.1	15.7	3	6648	T72
N4864	160-A12		12 56.80	28 14.9	5.1	14.8	1	6831	LMNS
								6902	G
								6769	TG76
	160-74		12 56.8	27 40.	34.2	15.4	3	5633	GR1
	-	RB244	12 56.8	27 54.	20.4	18.3	1	5584	T72
N4867	160-A13		12 56.83	28 14.5	4.7	15.5	1	4827	LMNS
								4669	G
	160-A14	RB268	12 56.83	28 20.8	8.4	15.6	3	7811	T72
	-	RB136	12 56.9	28 28.	14.7	16.5	3	9684	T73
	-	RB6	12 56.9	28 09.	6.1	16.2	1	6526	T72
								6589	G
	-	RB7	12 56.9	28 15.	3.9	17.2	3	6420	T72
	-	RB271	12 56.9	28 21.	8.1	16.8	3	7135	T73
N4865	160-A15	TT10	12 56.92	28 21.2	8.2	14.6	1	4655	LMNS
								4588	TT75
								4575	G
N4869	160-A16	TT11	12 56.97	28 11.0	3.9	14.9	1	6715	LMNS
								6894	G
								6801	TG76
	-	RB8	12 57.0	28 10.	4.5	16.3	3	5100	T72
								5086	G
	-	RB13	12 57.0	28 14.	2.4	16.6	3	7671	T72
								7550	G
	-	RB14	12 57.0	28 15.	2.7	16.3	1	6091	T72
	-	RB18	12 57.0	28 16.	3.2	16.6	3	6665	T72
								6885	G
	-	RB11	12 57.0	28 12.	3.0	17.5	1	7840	T73
	-	RB140	12 57.0	28 27.	13.4	17.4	1	7430	T73
	-	RB139	12 57.0	28 33.	19.3	16.9	3	7921	T73
I3967	160-A17		12 57.07	28 07.3	6.7	15.5	1	6937	K
								6887	G
								6777	TG76

TABLE I. (continued)

NGC/IC	Zw	Other	Ra (1950)	Dec (1950)	R (')	Mag	Morph	Vo	Ref
(1)	(2)	(3)	(4)	(5)	(6)	(7)	(8)	(9)	(10)
N4871	160-A18		12 57.08	28 13.7	1.3	15.1	3	7100	K
								6682	G
								6757	TG76
	-	RB22	12 57.1	28 19.	5.3	15.9	1	5588	T72
								5441	G
I3973	160-A19		12 57.10	28 09.4	4.5	15.2	3	4732	K
								4672	G
	-	RB26	12 57.1	28 19.	5.3	15.1	3	6916	T73
	-	RB234	12 57.1	28 04.	9.9	16.6	1	7841	T72
	-	RB21	12 57.1	28 21.	7.3	16.7	3	3660	T73
N4873	160-A20		12 57.13	28 15.1	1.5	15.4	3	5649	K
								5697	G
N4872	160-A21		12 57.15	28 13.0	0.9	15.3	3	6923	LMNS
								7021	K
								7184	G
								7258	TG76
N4874	160-A22	TT12	12 57.18	28 13.8	0.0	13.7	1	7183	LMNS
								7131	K
								6971	CR1
								7180	TT75
								7119	G
	160-76		12 57.2	28 54.	40.2	15.6	6	5342	CR2
I3990	160-77		12 57.2	29 10.	56.2	15.0	3	6208	K
I3991	160-78		12 57.2	29 12.	58.2	15.5	3	5914	GR1
	-	RB38	12 57.2	28 15.	1.2	16.5	3	6856	T73
								6812	G
	-	RB31	12 57.2	28 08.	5.8	17.2	3	6426	T73
	-	RB144	12 57.2	28 26.	12.2	17.1	1	5437	T73
N4875	160-A23		12 57.22	28 10.6	3.2	15.6	3	7870	T72
								7793	G
								7866	TG76
	160-A24	RB43	12 57.28	28 11.7	2.5	15.7	1	6812	T72
								6962	G
	-	RB40	12 57.3	28 13.	1.8	16.3	3	7920	T72
								7690	G
	-	RB42	12 57.3	28 14.	1.6	16.7	3	7663	T73
								7553	G
	-	G95	12 57.3	27 56.	17.9	.		6730	G
	-	RB45	12 57.3	28 16.	2.7	16.0	1	7001	T72
								6699	G
	-	RB46	12 57.3	28 14.	1.6	16.6	3	6771	T72
								6940	G
	160-79		12 57.3	27 58.	15.9	15.1	5	8219	K
								8324	G
	-	RB41	12 57.3	28 07.	7.0	16.3	1	3690	T72
	-	RB44	12 57.3	28 08.	6.0	17.2	3	17470	TT77
N4876	160-A25		12 57.32	28 11.0	3.4	15.1	1	6979	K
								6840	G
								6739	TG76
	160-A26	RB49	12 57.35	28 07.6	6.6	15.6	3	7916	T72
								7988	G
								8037	TG76
I3998	160-A27		12 57.37	28 14.6	2.6	15.6	3	9358	K
								9400	TG76
	-	RB55	12 57.4	28 12.	3.4	17.0	3	9842	T73
	160-80		12 57.4	32 18.	244.2	14.7		6844	TG76
	-	RB155	12 57.5	28 24.	11.0	16.1	3	7453	T72
								7560	G
	-	RB64	12 57.5	28 12.	4.6	16.1	3	7848	T73
								7747	G
	-	RB60	12 57.5	28 06.	8.9	17.2	3	7895	TT77
N4883	160-A28	TT36	12 57.52	28 18.2	6.3	15.2	3	7949	K
								8041	G
								8051	TG76
N4881	160-A29		12 57.55	28 31.0	17.9	14.7	1	6703	LMNS
								6725	TG76
N4892	160-81		12 57.6	27 10.	64.0	14.7	4	5881	K
	-	RB160	12 57.6	28 31.	18.1	16.9	3	7432	T73
	-	RB71	12 57.6	28 13.	5.6	17.9	3	5994	TT77
	-	RB68	12 57.6	28 13.	5.6	17.8	3	6949	TT77
	189-9		12 57.6	33 42.	328.2	15.2		7477	RC2
N4886	160-A30		12 57.65	28 15.3	6.4	15.1	1	6226	LMNS
								6492	G
	160-A31	TT13	12 57.67	28 04.6	11.3	15.7	2	6636	TT75
								6540	G
								6640	U
	-	RB74	12 57.7	28 18.	8.1	16.6	3	5931	T72
	-	RB77	12 57.7	28 15.	7.0	16.0	3	7816	T72
N4889	160-A32		12 57.70	28 14.7	6.9	13.0	1	6512	LMNS
								6505	G
								6521	TG76
I4011	160-A33		12 57.70	28 16.3	7.3	15.6	1	7115	T72
	-	G92	12 57.7	28 03.	12.8	15.8		6061	G
	-	G96	12 57.7	27 57.	18.2	16.3		6716	G
	-	TT25	12 57.7	28 31.	18.5	16.0		7259	TT75
	-	TT39	12 57.7	27 07.	67.2	.	5	23750	TT77
W	160-A34A	RB82	12 57.72	28 08.1	9.1	15.6	5	5121	T73
								5131	G
E	160-A34B	RB83	12 57.72	28 08.1	9.1	16.8	3	9878	T72
I4012	160-A35		12 57.72	28 20.8	10.0	15.7	1	7349	T72
								7154	G
								7248	TG76

TABLE I. (continued)

NGC/IC (1)	Zw (2)	Other (3)	Ra (1950) (4)	Dec (1950) (5)	R (') (6)	Mag (7)	Morph (8)	Vo (9)	Ref (10)
	160-A36	RB167	12 57.75	28 26.2	14.5	15.6	1	6774	LMNS
	-	RB87	12 57.8	28 21.	10.9	15.8	3	7394	K
								7552	G
	160-82	TT40	12 57.8	27 39.	35.8	15.6	5	10871	GR1
								11183	TT77
	160-83		12 57.8	29 06.	52.8	15.4	3	7399	GR1
I4021	160-A37		12 57.83	28 18.5	9.8	15.6	1	5804	LMNS
								5553	G
N4894	160-A38		12 57.87	28 14.2	9.1	15.7	3	4560	T72
								4590	G
N4898E	160-A39A		12 57.88	28 13.5	9.3	16.4	1	6513	T72
N4898W	160-A39B		12 57.88	28 13.5	9.3	14.7	1	6950	LMNS
								6768	T72
								6755	G
								6812	TG76
N4895	160-A40		12 57.88	28 28.1	17.0	14.3	4	8422	LMNS
								8264	G
								8401	TG76
	-	RB91	12 57.9	28 20.	11.4	16.3	3	6179	K
								6146	T73
								6215	G
	-	RB94	12 57.9	28 13.	9.5	16.6	3	5146	T72
								5098	G
I4026	160-A41		12 57.95	28 18.9	11.4	15.5	3	8162	T72
								8131	G
								8198	TG76
	160-84		12 58.0	26 56.	78.6	15.2		7212	GR1
I4032	160-85		12 58.0	29 08.	55.3	15.4	3	6787	GR1
	-	TT41	12 58.0	27 47.	28.9	16.0	1	7849	TT77
	-	TT42	12 58.0	27 47.	28.9	16.0	9	7467	TT77
	-	RB99	12 58.1	28 14.	12.2	16.0	3	6936	T72
								6883	G
	-	RB100	12 58.1	28 15.	12.2	15.9	3	7753	T72
								7686	G
	-	G97	12 58.1	28 02.	17.0	16.5		6716	G
	160-86	TT43	12 58.1	27 55.	22.4	15.4	6	7508	CR1
								7481	TT77
N4896	160-87		12 58.1	28 37.	26.2	15.1	3	5836	LMNS
	160-A42		12 58.18	28 24.9	17.3	15.7		5536	TG76
I842	160-88		12 58.2	29 17.	64.6	14.6	5	7193	GR1
	-	RB110	12 58.2	28 17.	13.9	16.2	3	7587	T72
I4040	160-A43	TT14	12 58.22	28 19.6	14.9	15.1	5	7527	LMNS
								7759	CR2
								7644	TT75
								7613	TG76
N4906	160-A44		12 58.25	28 11.6	14.3	15.2	1	7478	T72
								7438	G
								7510	TG76

NGC/IC (1)	Zw (2)	Other (3)	Ra (1950) (4)	Dec (1950) (5)	R (') (6)	Mag (7)	Morph (8)	Vo (9)	Ref (10)
I4041	160-A45		12 58.27	28 15.8	14.5	15.7	1	7087	T73
								6972	G
	160-89		12 58.3	28 36.	26.7	15.6	2	8008	GR1
I4042	160-A46		12 58.30	28 14.2	14.8	15.5	3	6243	K
								6603	TG76
	-	RB113	12 58.3	28 14.	14.8	15.8	3	8056	K
	-	RB116	12 58.3	28 22.	16.9	16.3	3	6621	T72
	-	TT15	12 58.3	28 47.	36.3	16.0		8970	TT75
	-	TT16	12 58.3	28 41.	31.0	17.8		6314	TT75
	-	RB119	12 58.4	28 11.	16.4	16.2	3	8692	T72
								8638	G
I4045	160-A47		12 58.40	28 21.5	17.9	15.1	1	6542	LMNS
								6938	G
								6865	TG76
N4907	160-A48		12 58.4	28 25.5	19.9	14.6	5	5883	LMNS
	160-90		12 58.4	27 40.	37.5	15.5	5	6932	GR1
N4908	160-A49		12 58.45	28 18.6	17.5	14.9	1	8853	LMNS
								8850	TG76
I4051	160-A50		12 58.48	28 16.5	17.4	14.8	1	4947	LMNS
								4922	G
	160-91	A14	12 58.5	28 38.	29.8	14.9	3	7695	K
N4911	160-A51	TT17	12 58.50	28 03.5	20.3	13.7	5	8021	LMNS
								7898	TT75
								7868	G
								7831	TG76
	-	RB122	12 58.5	28 06.	19.1	17.2	3	7215	T72
	160-A52	RB124	12 58.67	28 10.0	20.1	15.6	5	6917	T73
								6860	G
	160-92	G100	12 58.7	28 05.	21.9	15.7	2	5986	GR1
								5703	G
	-	RB128	12 58.7	28 18.	20.5	17.0	1	6925	T73
	160-93		12 58.8	28 04.	23.6	15.7	3	6522	GR1
								6820	G
	-	RB129	12 58.8	28 11.	21.6	16.4	1	6015	T73
								5838	G
N4919	160-94		12 58.9	28 04.	24.8	14.9	4	7098	K
								7253	G
								7278	TG76
N4921	160-95		12 59.0	28 08.	24.8	13.7	5	5474	LMNS
								5344	G
								5486	TG76
								5331	TT77
N4922S	160-96A	TT26	12 59.0	29 35.	84.6	14.2	7	7372	LMNS
								7232	TT75
								7251	TG76
N4922N	160-96B	TT18	12 59.0	29 35.	84.6	.		7027	TT75

TABLE I. (continued)

NGC/IC (1)	Zw (2)	Other (3)	Ra (1950) (4)	Dec (1950) (5)	R (') (6)	Mag (7)	Morph (8)	Vo (9)	Ref (10)
	–	RB133	12 59.0	28 16.	24.1	16.5	1	7482	T73
N4923	160-97		12 59.1	28 06.	26.6	14.7	1	5446	K
	160-98	TT46	12 59.1	28 57.	50.1	15.3	5	8922	GR1
								8772	TT77
I843	160-99	A15	12 59.2	29 24.	75.1	14.8	1	7518	K
								7416	TG76
	–	TT47	12 59.2	28 25.	28.9	17.0	3	5387	TT77
	–	TT48	12 59.2	28 25.	28.9	18.0	1	6032	TT77
	160-100		12 59.4	28 09.	29.7	15.5	1	7626	GR1
	160-101		12 59.4	28 22.	30.4	15.2	3	5928	GR1
I4088	160-102		12 59.4	29 19.	71.4	14.8		7027	GR1
N4926	160-103		12 59.5	27 53.	37.1	14.1	1	7676	LMNS
								7900	K
	160-104		12 59.6	28 03.	33.8	15.4	4	7213	CR2
N4927	160-105	TT49	12 59.6	28 16.	32.1	14.8	1	7572	K
								7573	TT77
	160-106		12 59.7	27 55.	38.3	15.1	5	7186	LMNS
	160-107	A16	12 59.7	29 31.	84.0	14.9	3	7285	K
								7431	CR1
								7426	TG76
	160-108		12 59.8	28 29.	37.8	15.5	7	8323	CR2
	160-109		12 59.8	28 40.	43.4	15.5	3	7625	GR1
	160-110		13 00.0	28 30.	40.6	15.2	3	5733	GR1
	160-111		13 00.0	28 32.	41.4	15.7	2	7149	GR1
I4106	160-112		13 00.2	28 22.	40.7	15.5	4	7454	GR1
N4929	160-113		13 00.3	28 18.	41.4	14.9	1	6353	CR2
	160-114		13 00.3	28 39.	48.3	15.6	5	7454	GR1
	–	TT50	13 00.3	28 24.	42.4	.	1	49250	TT77
	160-115		13 00.4	28 07.	43.1	15.1	2	8180	GR1
I4111	160-116		13 00.5	28 20.	44.3	15.7	3	7904	GR1
	160-117		13 00.6	26 47.	98.0	15.7		5970	GR1
N4931	160-118		13 00.6	28 17.	45.3	14.4	3	5839	K
	160-119		13 00.8	28 50.	59.9	15.2	2	6931	CR2
N4934	160-120		13 00.9	28 17.	49.3	15.0	5	6104	GR1
	160-121		13 01.0	26 49.	98.9	15.5		6729	GR1
I4149	130-5		13 01.2	22 34.	344.1	15.5		7045	TG79
	130-4		13 01.3	26 21.	125.5	15.7		11206	GR1
N4943	160-122		13 01.4	28 21.	56.2	15.6	3	5751	GR1
	–	TT51	13 01.4	29 29.	93.4	.		50013	TT77
I4133	160-123		13 01.5	28 15.	57.1	15.4	1	6342	GR1
N4944A	160-124A		13 01.5	28 28.	58.8	13.3	3	7013	LMNS
	160-125		13 01.8	28 31.	63.4	15.4	3	5984	GR1
	–	TT19	13 01.9	28 44.	69.2	16.0	1	7787	TT75
	160-126		13 02.0	26 56.	100.8	15.3		10820	GR1
	160-127		13 02.0	27 34.	75.3	15.5		5627	GR1
	160-128		13 02.0	29 05.	81.5	15.3		8066	CR1

NGC/IC (1)	Zw (2)	Other (3)	Ra (1950) (4)	Dec (1950) (5)	R (') (6)	Mag (7)	Morph (8)	Vo (9)	Ref (10)
N4952	160-129		13 02.6	29 23.	99.3	13.6	1	5886	LMNS
	130-6	A17	13 02.8	26 13.	142.2	15.0	7	6542	K
N4957	160-130		13 02.8	27 50.	78.1	14.2	1	6995	K
I846	130-7		13 02.9	23 22.	301.8	15.5		10122	TG79
	–	MK62	13 02.9	30 32.	157.1	.		9905	RC2
	160-132		13 03.0	29 34.	110.8	15.5		7176	GR1
N4961	160-134	TT21	13 03.3	28 00.	82.1	13.5	5	2579	LMNS
								2588	TT75
	160-135		13 03.6	28 51.	92.4	15.5		8010	GR1
	160-136		13 03.6	29 33.	115.7	15.0		8000	GR1
	130-8	A18	13 03.8	25 43.	174.8	14.9		7387	K
N4966E	160-137A		13 03.9	29 20.	110.4	13.9	5	7098	K
N4966W	160-137B		13 03.9	29 20.	110.4	.		7181	GR2
	–	A1303+33	13 04.0	33 14.	312.8	.		7777	RC2
	160-138		13 04.1	27 26.	103.5	15.7		7861	GR1
	160-139		13 04.2	29 06.	106.1	15.0		4854	GR1
	–	A1304+28	13 04.3	28 08.	94.3	.		6905	RC2
N4971	160-140		13 04.5	28 48.	102.4	15.0	1	6394	K
	160-141		13 04.8	28 18.	100.8	15.5		6654	GR1
E	160-142A	CT38	13 05.0	26 59.	128.1	15.5	1	11517	TG73
W	160-142B		13 05.0	26 59.	128.1	.		11301	GR2
	160-143		13 05.2	27 45.	110.1	15.7		6667	GR1
N4979	130-9		13 05.2	25 05.	217.3	15.3		6596	TG79
	160-144	CT39	13 05.6	27 01.	133.5	15.6	1	10352	TG73
	160-145		13 05.6	28 58.	119.4	15.4		7730	GR1
	160-146		13 05.8	27 46.	117.5	15.4		7385	GR1
N4983	160-147		13 06.0	28 35.	118.3	14.9		6647	GR1
I4202	130-12		13 06.0	24 58.	228.7	15.2		7295	TG79
	160-148		13 06.5	28 27.	123.8	14.3		5986	GR1
	160-149		13 06.6	28 18.	124.5	15.6		7276	GR1
	160-150		13 06.6	29 18.	139.5	15.7		9590	GR1
	130-13		13 06.7	22 41.	356.9	15.6		10325	TG79
	160-151	A19	13 06.9	29 38.	152.9	15.1		6534	K
								6390	CR1
N5000	160-152		13 07.4	29 10.	145.7	14.0	5	5643	K
								5729	CR1
I854N	130-14A		13 07.4	24 51.	244.8	15.1		7117	TG79
I854S	130-14B		13 07.4	24 51.	244.8	.		7187	TG79
I4210	160-155		13 08.4	29 59.	180.8	15.3		6450	GR2
N5004	160-157		13 08.7	29 54.	181.2	14.3	1	6984	K
N5004A	160-156		13 08.7	29 50.	179.1	15.3	5	7190	K
N5012	130-16		13 09.1	23 12.	342.1	13.6		2566	TG76
	160-158		13 09.3	31 46.	264.2	14.6	3	7034	TG76
	160-159	CT41	13 09.7	27 35.	170.4	15.0	1	6141	TG73
N5016	130-19		13 09.7	24 21.	287.3	14.3		2769	TG76
	160-160	A20	13 09.9	26 57.	185.7	14.6	5	877	K

TABLE I. (continued)

NGC/IC	Zw	Other	Ra (1950)	Dec (1950)	R (')	Mag	Morph	Vo	Ref
(1)	(2)	(3)	(4)	(5)	(6)	(7)	(8)	(9)	(10)
	160-161		13 10.0	28 47.	172.2	15.7		6938	GR2
	130-20		13 10.2	23 06.	354.5	14.8		2592	TG76
N5025	160-162		13 10.4	32 04.	287.0	14.6	5	6394	TG76
	160-163	CT40	13 10.6	27 25.	184.6	15.7	5	6877	TG73
	160-165	CT42	13 11.0	28 01.	183.3	15.7	3	6270	TG73
N5032	160-166		13 11.0	28 04.	183.0	13.6		6536	TG76
	130-21		13 11.3	25 25.	253.4	15.4		7168	TG79
	130-22		13 11.4	23 31.	341.7	15.7		3472	TG79
N5041	160-168		13 12.2	30 58.	255.6	14.2	5	7471	TG76
I860	130-23		13 12.6	24 53.	288.3	14.8		3871	TG76
N5052	160-171		13 13.2	29 55.	233.1	14.6	4	6773	TG76
	-	A1313+25	13 13.5	25 42.	265.8	.		945	RC2
N5056	160-173		13 13.8	31 12.	280.4	13.6		5481	TG76
	130-24		13 13.8	25 40.	270.2	15.0		3790	TG79
	160-174		13 13.9	30 31.	258.0	14.9		14839	TG76
N5057	160-176		13 14.1	31 17.	286.5	14.6		5856	TG76
N5056	160-181		13 15.2	31 20.	299.5	14.3		5732	TG76
N5074	160-183		13 16.1	31 44.	323.4	14.7		5720	TG76
N5081	160-192		13 16.8	28 46.	260.6	14.3	5	6731	TG76
N5089	160-194		13 17.3	30 31.	296.6	14.4		2190	TG76
	160-202		13 18.0	31 47.	344.3	14.9		5183	TG76
	160-208		13 19.0	31 39.	350.0	15.0		7121	TG76
	161-30		13 19.3	31 27.	346.6	14.8		5088	TG76
	160-31		13 19.4	31 30.	349.3	14.9	5	7272	TG76
N5116	161-36		13 20.6	27 15.	316.4	13.7		2859	TG76
N5117	161-37		13 20.6	28 35.	309.7	14.5		2465	TG76
I4234	161-38		13 20.7	27 23.	316.1	14.9		10377	TG76

References to Table I

CR1. Chincarini and Rood (1972a).
CR2. Chincarini and Rood (1972b).
CR3. Chincarini and Rood (1976).
G. Gunn, this paper.
GR1. Gregory (1975a).
GR2. Gregory (1975b).
K. Kintner (1971).
LMNS. Lovasich *et al.* (1961).
RC2. de Vaucouleurs, de Vaucouleurs, and Corwin (1976).
T72. Tifft (1972).
T73. Tifft (1973).
TG73. Tifft and Gregory (1973).
TG76. Tifft and Gregory (1976).
TG79. Tifft and Gregory (1979).
TT75. Tifft and Tarenghi (1975).
TT77. Tifft and Tarenghi (1977).
U. Ulrich (1976).

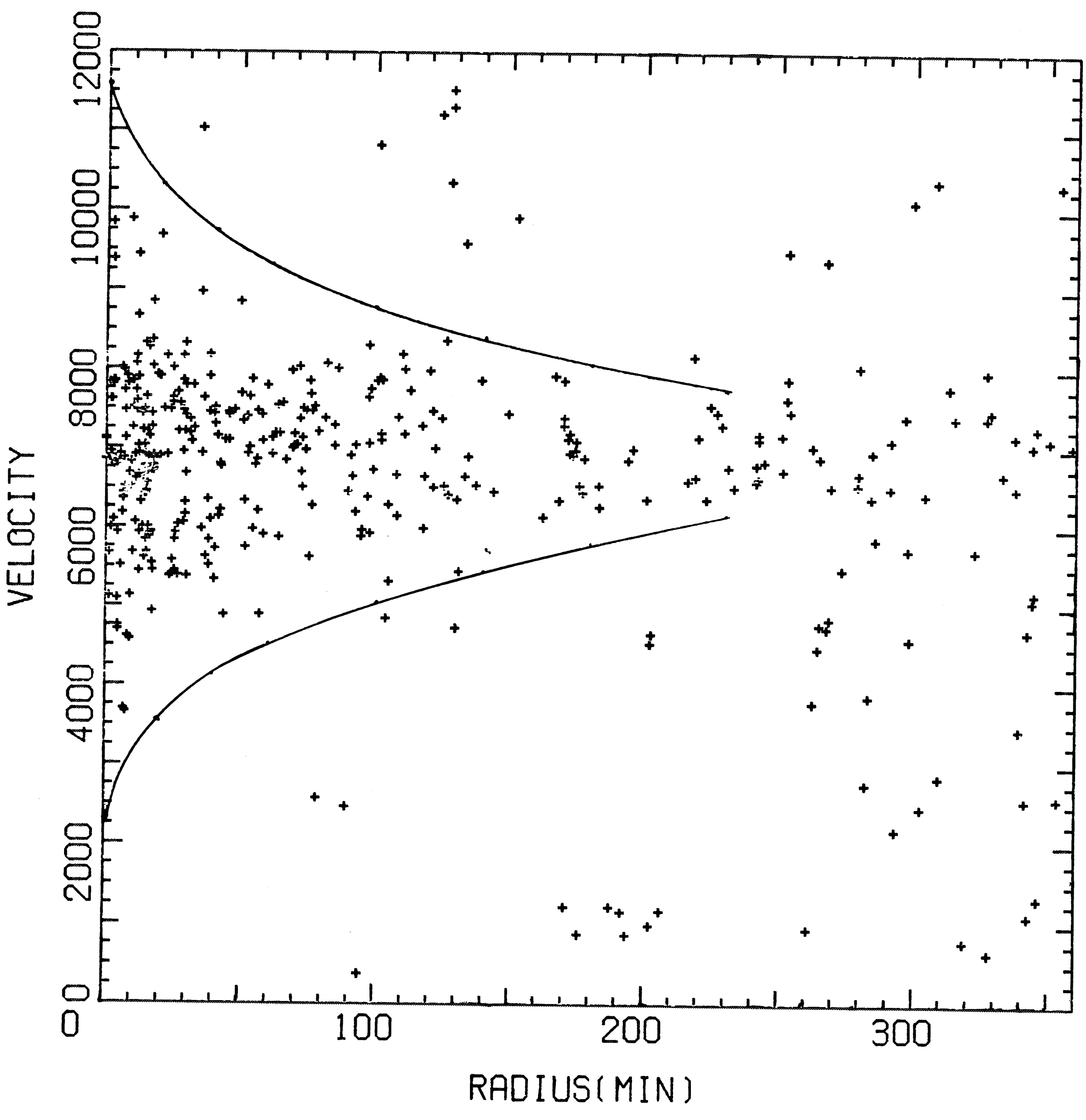

FIG. 1. Distribution of radial velocities in Coma as a function of distance from the cluster center.

TABLE II. Velocity-dispersion profile.

r (arcmin)	σ (km s^{-1})
1.5	1137
4.9	1243
9.2	1438
12.9	997
15.4	741
19.2	1149
25.7	1033
32.9	891
41.6	931
51.5	850
65.3	571
82.5	658
100	807
124	758
158	587

termined by taking all the cluster members from Table I and binning them radially in groups of 20. These dispersions have not been corrected for any measurement error, but if the oft-quoted uncertainty of 100 km s^{-1} were used, any correction would be less than 2%.

As was first shown by RPKK, the velocity dispersion falls from ~1000 km s^{-1} at the cluster center to about half this value at $R = 3°$. A secondary rise near $R = 2°$ noted by Gregory and Thompson (1978) is also seen but is not very significant.

III. SURFACE-DENSITY PROFILE

An accurate determination of the surface-density profile is constrained by two conflicting requirements. To achieve high statistical accuracy one would like to make galaxy counts to a faint limiting magnitude, but doing so increases the contamination by background galaxies. We have therefore formed a composite profile by the following method. In the central regions, the profile is determined from counts to a faint limiting magnitude where background contamination is not a serious problem. At large radii we restrict ourselves to a bright limiting magnitude and select cluster members on the basis of radial velocities.

a) Faint Sample

To determine the inner surface-density profile we use the photometric survey of Godwin and Peach (1977), who list all galaxies in a 1.22° square field centered on Coma down to a limiting magnitude $m_v = 19.5$; corrections to this survey as noted by Thompson and Gregory (1980) have been included. When needed elsewhere, we have converted the Zwicky magnitudes by the relation $m_p = m_v + 0.94$.

The Godwin and Peach survey has been analyzed by Sarazin (1980) using a maximum-likelihood technique, and he has determined, among other quantities, the cluster center. Since NGC 4874 lies within 1σ of the center so determined, we have, for simplicity, adopted its position as the cluster center ($\alpha = 12^{\rm h}57^{\rm m}\!.18$, $\delta = 28°13^{\rm m}\!.8$). Using the same survey, Quintana (1979) illustrates the effect of varying the position of the center on the cluster profile.

To determine the surface-density profile, the galaxies are binned in annular rings whose width is varied so as to keep the number of galaxies in each bin approximately constant. Since the cluster profile is known to vary approximately as $\mu \sim \mu_0[1 + (r/r_c)^2]^{-1}$, the bin boundaries are spaced uniformly in the quantity $\ln[1 + (r/r_c)^2]$. We take an *a priori* value of 9′ for the core radius and set the number of bins so as to keep approximately 20 galaxies per bin.

Because of resolution effects, the average measured surface density in a given bin may underestimate the true density. This effect is corrected as follows. If ΔN is the number of galaxies between r_1 and r_2, the true surface density is estimated to be

$$\bar{\mu}\left(\frac{r_1 + r_2}{2}\right) = \frac{\Delta N}{\pi(r_2^{\,2} - r_1^{\,2})} \times \left(\frac{r_2^{\,2} - r_1^{\,2}}{\ln[1 + (r_2/r_c)^2] - \ln[1 + (r_1/r_c)^2]} \times [r_c^{\,2} + \tfrac{1}{4}(r_1 + r_2)^2]^{-1}\right). \quad (1)$$

The correction term in the large parentheses never exceeds 5%.

Although the Godwin and Peach sample is complete to a limit of $m_v = 17.5$, we have elected to impose a brighter limit of $m_v = 16.5$ since (a) background corrections are less uncertain, and (b) going to a limit of $m_v = 17.5$ does not significantly improve the statistical scatter of the profile. The background correction has been estimated using data from Abell (1977) and Oemler

TABLE III. Surface-density profile.

$R_{\rm min}$ (arcmin)	$R_{\rm max}$ (arcmin)	N	Background	μ (galaxies deg^{-2})
		a. $m_v \leqslant 16.5$ (GP sample)		
0.	5.0	23	0	1100
5.0	7.6	20	0	693
7.6	10.1	19	0	498
10.1	12.6	21	0	417
12.6	15.2	25	0	378
15.2	18.1	17	0	191
18.1	21.4	18	1	152
21.4	25.0	22	1	141
25.0	29.0	28	1	137
29.0	33.6	28	2	102
		b. $m_p \leqslant 15.7$ (radial velocity sample)		
0	8.2	21		411
8.2	13.7	16		153
13.7	20.2	22		114
20.2	28.5	14		39.8
28.5	39.3	22		34.3
39.3	53.6	21		18
53.6	72.8	26		12.2
72.8	98.6	26		6.7
98.6	133	27		3.8
133	180	22		1.7

(1974); we estimate $\mu_b \sim 10$ galaxies deg^{-2} with an uncertainty of 50%.

The resulting surface-density profile is listed in Table III (a).

b) Bright Sample

To determine the cluster profile at large radii, we restrict ourselves to a limiting magnitude $m_p \leqslant 15.7$ and $R < 3°$. As we have noted earlier, Tifft and Gregory (1976) have measured redshifts for virtually all objects in this sample. Selecting only cluster members, this sample has been binned in the same manner as the faint sample, keeping ~ 20 galaxies per bin, and correcting for resolution effects via Eq. (1). These corrections are now larger, being 24% for the innermost bin. The resulting profile is listed in Table III (b).

By selecting galaxies according to radial velocities, most contamination by foreground and background galaxies is eliminated. However, there may still be contamination by supercluster galaxies projected onto Coma but not dynamically bound to it. The magnitude of this contamination can be estimated as follows. In the zone $3° < R < 6°$ there are 21 galaxies in the complete sample of Tifft and Gregory (1976) to a limit $m_p < 15.0$ with velocities in the range $6000 < V < 8000$ km s^{-1}. Using the luminosity function of cluster members in the zone $R < 3°$, we would expect to find 74 objects to a limit $m_p \leqslant 15.7$ in the outer zone, for a mean density of 0.87 galaxies deg^{-2}. Some of these objects might be expected to be cluster members, so this number provides an upper limit to the estimated supercluster contamination. From Table II (b) it is seen that only the last point might be seriously affected.

IV. SEGREGATION EFFECTS IN COMA

a) Luminosity Segregation

The question of whether or not the distribution of galaxies in Coma depends on luminosity has been the object of some attention. Zwicky (1957) argued, on the basis of counts of different limiting magnitudes, that considerable segregation does exist, and he took this as evidence for energy equipartition. However, RPKK showed that this segregation largely disappears when proper account is made for the background correction to Zwicky's faintest sample. It is now generally accepted that there is no significant segregation in the large-scale distribution of galaxies in Coma.

Somewhat more controversial is the evidence for segregation in the core of Coma. Quintana (1979) has used the Godwin and Peach (1977) survey to measure the core radius as a function of limiting magnitude and does find an increase in core radius by perhaps as much as a factor of 2 between $m_v = 15$ and $m_v = 18.5$. Sarazin (1980), using the same data but a different technique, arrives at the opposite conclusion, namely that the evidence for segregation is weak. However, in his fitting method he has attempted to solve for the density of background galaxies and arrives at numbers that are typically too large by a factor of 4 as compared with the values found here, thus causing him to systematically underestimate the core radius.

TABLE IV. Velocity dispersion vs magnitude.

m_1	m_2 ($m_1 < m \leqslant m_2$, $r < 30'$)	n	σ
	$\leqslant 15.0$	21	1085
15.0	15.5	31	1081
15.5	16.0	37	984
16.0	16.5	24	1176
$16.5 \leqslant$		32	1250

If the surface-density distribution depends on luminosity, there should be a corresponding dependence of velocity dispersion on magnitude. To check for such an effect we have computed the velocity dispersion for galaxies binned into different magnitude intervals. We restrict ourselves to $R < 30'$ where the fainter members of Coma are most completely surveyed. In Table IV we list the values so determined. It is seen that any dependence of dispersion on magnitude is rather minimal. However, the range in luminosity is only three magnitudes, and in particular does not extend to the faintest galaxies where the differences in surface-density distribution are strongest.

Because of the possible evidence for luminosity segregation in the core of Coma, it should be kept in mind that our surface-density profiles refer to a limiting magnitude $m_v = 16.5$. However, since this is also approximately the limit to which radial velocities are available in the core, we will at least be consistent when the time comes to fit dynamical models to the core region.

b) Morphological Segregation

The dependence of surface density and velocity dispersion on morphological type in clusters has been recognized for some time (Oemler 1974) and Coma is no exception. We shall restrict ourselves to a subset of the galaxies in Table I for which $m_p \leqslant 15.7$ and $R < 1°$. Of the 125 cluster members, all but one has a morphological type. With this small sample it is no longer meaningful to define a surface-density profile for each morphological type. Rather, we characterize the density distribution by the median radius $r_{1/2}$ inside of which one-half the galaxies of each type are located. In Table V we list the value of $r_{1/2}$ along with the overall velocity dispersion for the three morphological types E, S0, and Sp (intermediate types have been assigned to give roughly equal numbers in each group).

A clear trend is present. The morphological types can be ordered E–S0–Sp as measured both by decreasing degree of concentration and by increasing velocity dispersion. Later we shall consider the dynamical implications of segregation from a more quantitative point of view.

TABLE V. Radial distribution and velocity dispersion vs morphological type.

Type	Observed %	Observed $r_{1/2}$	Observed $\sigma/\bar{\sigma}$	Method 1 %	Method 1 $r_{1/2}$	Method 1 $\sigma/\bar{\sigma}$	Method 2 %	Method 2 $r_{1/2}$	Method 2 $\sigma/\bar{\sigma}$
E + E/S0	38	17.3	0.87	—	16.0	0.94	33	16.6	0.94
S0	36	21.0	1.03	—	22.5	1.00	36	22.5	1.00
S0/Sp + Sp	26	31.5	1.10	—	31.0	1.08	31	30.0	1.07

Total No. of galaxies: 124

V. DYNAMICAL MODELS

a) Assumptions

As usual, we begin by making a number of simplifying assumptions about the cluster properties.

1) Spherical Symmetry

Although Coma is noticeably elongated, we are interested primarily in the radial structure, which should be adequately represented by spherically symmetric models.

2) Dynamical Equilibrium

This assumption is probably reasonable for Coma inside $R = 3°$. A galaxy at this distance will have traversed a cluster radius three times during the age of the universe.

3) Single Component

In making this assumption, we presume that any "dark matter" in the cluster is distributed like the galaxies. Later we consider the effects of relaxing this assumption.

b) Distribution Function

The central problem in construcing dynamical models for clusters is choosing a proper form for the distribution function $f(E,J)$, where E is the total energy and J the total angular momentum of a particle. Since two-body relaxation is not likely to have yet dominated the cluster dynamics (except possibly in the center), the distribution ought to reflect the initial chaotic conditions from which a cluster formed. If cluster collapse were sufficiently chaotic, violent relaxation (Lynden-Bell 1967) would effectively randomize galaxy motions and drive the cluster towards a Maxwell-Boltzman distribution, but with no mass segregation. At the opposite extreme, if a cluster forms by the smooth accretion of material onto a central core, little randomization will occur, and the cluster will tend towards a polytropic structure with the galaxies in predominately radial orbits (Gott 1975; Gunn 1977). In practice some intermediate combination is likely to occur.

Motivated by these considerations, we have explored four possible distribution functions:

$$f_1 = A_1(e^{-E/\sigma^2} - 1)e^{-J^2/2J_0^2}, \quad (2a)$$

$$f_2 = A_2(-E)^{\beta}e^{-J^2/2J_0^2}, \quad (2b)$$

$$f_2 = A_3(e^{-E/\sigma^2} - 1)J^{-\gamma}, \quad (2c)$$

$$f_4 = A_4(-E)^{\beta}J^{-\gamma}. \quad (2d)$$

It is seen that these functions simply combine two possible forms each for the energy and angular-momentum dependence. For the energy dependence we allow for either a lowered Gaussian (with characteristic energy σ^2) or a polytrope (with power-law index β). For the angular-momentum dependence we allow for two extreme cases of anisotropy. The term $\exp(-J^2/2J_0^2)$ produces models with orbits that are isotropic in the center and radial at the edge; J_0 is the cutoff angular momentum. The term $J^{-\gamma}$ produces a more uniform anisotropy, and in fact yields a constant ratio of tangential to radial velocity dispersions (which depends on the parameter γ). Function f_1 is a King-Michie distribution, first introduced by Michie (1963) to describe the structure of global clusters. In the limit $J_0 \to \infty$ the isotropic King (1966) models are recovered. The isotropic forms of either f_2 or f_4 ($J_0 \to \infty$, $\gamma \to 0$) yield standard polytropes of index $n = \beta + 3/2$ (Chandrasekhar 1939).

c) Scaling Laws

We introduce the scale quantities σ, r_s, and ρ_0 as the characteristic velocity, radius, and density, respectively. In keeping with the traditional definition of core radius, they are related by

$$4\pi G\rho_0 r_s^2 = 9\sigma^2. \quad (3)$$

For King models only, r_s is the radius at which the surface density falls to one-half its central value. For other models, r_s is simply a formal scale radius with no such simple interpretation (indeed, for some models the central density is either infinite or not even defined).

The physical meaning associated with each dimension depends on the specific distribution function. The following dimensionless quantities are defined:

(1) The potential W is in units of σ^2 and is defined to be zero at the edge of a cluster and positive within.

(2) The energy E is in the units of σ^2 and is defined to be positive for objects bound to a cluster.

(3) The radius r is in units of r_s.

(4) The density ρ is in units of ρ_0.

(5) The radial and tangential velocities v and h are in units of σ.

(6) The angular momentum J is in units of σr_s.

With these dimensions we have

$$E = W - \tfrac{1}{2}v^2 - \tfrac{1}{2}h^2, \quad J = hr.$$

For functions f_1 and f_2 we have a characteristic angular momentum $J_0 = \sigma r_t$, where r_t is defined to be the transition radius (identical with the definition of Gunn and Griffith 1979).

d) Physical Quantities

At any given radius in the cluster we can compute the following quantities:

$$\rho = \int f\, d^3v, \tag{4a}$$

$$\rho\langle v^2\rangle = \int f v^2\, d^3v, \tag{4b}$$

$$\rho\langle h^2\rangle = \int f h^2\, d^3v, \tag{4c}$$

where integrals are over the domain $0 < \frac{1}{2}(v^2 + h^2) < W$ and W is the potential at radius r. In general, these quantities depend explicitly on r as well as implicity through the potential W. These integrals can also be written in the alternative forms:

$$\rho = 4\pi \int dv \int f(E,J) h\, dh, \quad \begin{matrix} 0 < h < (2W - v^2)^{1/2} \\ 0 < v < (2W)^{1/2} \end{matrix}, \tag{5a}$$

$$= 4\pi \int dE \int \frac{f(E,J)\, J\, dJ}{r^2[2(W - E - J^2/2r^2)]^{1/2}}, \quad \begin{matrix} 0 < J < r[2(W-E)]^{1/2} \\ 0 < E < W \end{matrix}, \tag{5b}$$

etc. The constants A_1 through A_4 in Eqs. (2a)–(2d) are normalized such that $\rho = \rho_0$ at some specified value of r (typically $r = 0$). The evaluation of these integrals for each of the four distribution functions is done in the Appendix.

e) Poisson's Equation

A self-consistent dynamical model must satisfy Poisson's equation, $\nabla^2\Phi = 4\pi G\rho$. For our dimensionless variables with the scaling relation of Eq. (3) we get

$$\frac{1}{r^2}\frac{d}{dr}\left(r^2\frac{dW}{dr}\right) = -9\rho. \tag{6}$$

Since ρ is known explicitly in terms of W and r, this equation is easily integrated. The initial conditions are $W = W_0$ and $dW/dr = 0$ at $r = 0$. For some models the central density is formally infinite, and for these cases it is necessary to begin the integrations at some inner radius r_i with initial conditions $W = W_i$, $dW/dr = 9M_i/4\pi r_i^2$. M_i is the dimensionless mass inside r_i. W_i and M_i can usually be estimated from the known asymptotic behavior of ρ and W at small r.

Equation (6) can be readily integrated by standard techniques. The cluster edge is normally reached at a finite radius where the density reaches zero. Once the density and potential are known as a function of radius, the radial and tangential velocity dispersions can be computed and the relevant physical quantities then projected onto the plane of the sky.

f) Central Massive Objects

An object placed in the center of a cluster which is sufficiently massive (such as a cD galaxy) can distort the profile of the cluster core. In this case the procedure for integrating Eq. (6) is modified. We again begin by integrating at an inner radius r_i with the initial conditions $W_i = W_0 + 9M_i/4\pi r_i$, $dW/dr = 9M_i/4\pi r_i^2$. It is now necessary to specify the distribution function f in the domain $E > W_0$, i.e., for objects which are bound to the central mass. We have allowed for two extreme possibilities, one in which f continues unaltered for $E > W_0$ and the other in which $f = 0$. We shall refer to these cases as the "filled center" and "empty center" cases, respectively.

VI. MODEL CHARACTERISTICS

With four different distribution functions and a host of free parameters, models with a wide range of characteristics can easily be constructed. In this section we illustrate some of the features of these models, but restrict ourselves to those which might bear some resemblance to actual clusters. For convenience we assign names to each of the distribution functions.

a) $f_1 = [\exp E - 1] \exp(J^2/2J_0^2)$ (King-Michie)

The scaling parameters are selected such that ρ_0 is the central density and σ is the characteristic velocity dispersion in the distribution function. The available free parameters in a dimensionless model are the central potential W_0 and the transition radius r_t. For this distribution function only we have also explored the effects of a central massive object with mass M_i; M_i will always refer to the total mass inside $0.1r_s$.

Figure 2 illustrates the effect of varying these three parameters on the surface-density and velocity-dispersion profiles. In Figs. 2(a) and 2(b), the standard isotropic King models ($r_t = \infty$, $M_i = 0$) are shown. All these models terminate at a finite radius which increases with W_0. The velocity dispersion is constant to well beyond the core region and then falls smoothly to zero as the cluster edge is approached. We note that the oft-used approximation $\mu \propto \mu_0[1 + (r/r_s)^2]^{-1}$ is a reasonable approximation to the $W_0 = 8$ model out to $10r_s$.

The effects of anisotropy on the surface density are shown in Figure 2(c). Here we plot two models, one which is isotropic ($W_0 = 8$, $r_t = \infty$) and one with a transition radius $r_t = 12$ (W_0 has been increased slightly to better match the interior profile). The two profiles are virtually identical over the range plotted, with the aniso-

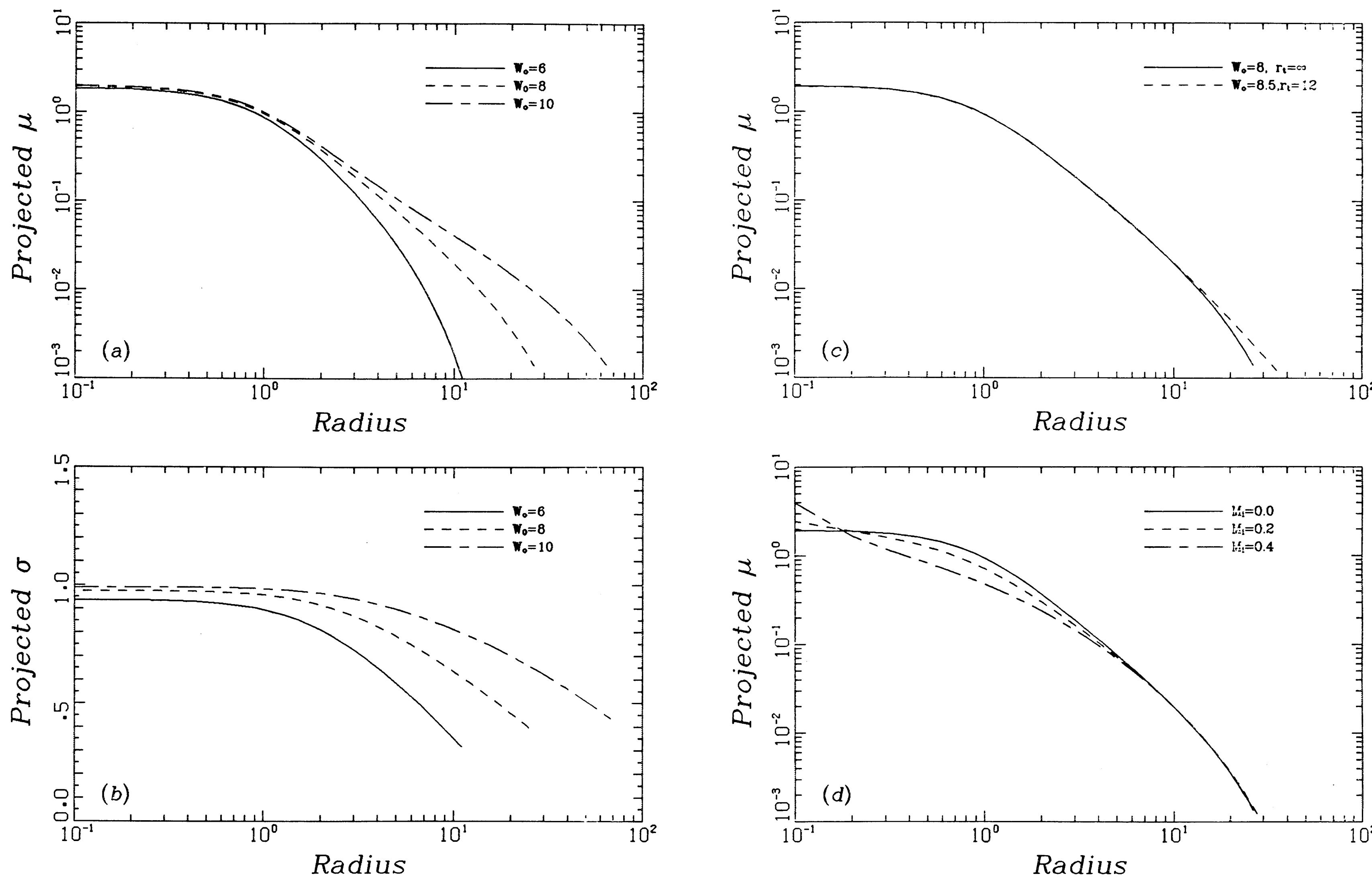

FIG. 2. Properties of King-Michie models. (a) Projected surface-density profile showing effects of varying central potential W_0. (b) Projected velocity-dispersion showing effects of varying W_0. (c) Same as (a) but varying the transition radius r_t. (d) Same as (a) but varying the central mass M_t.

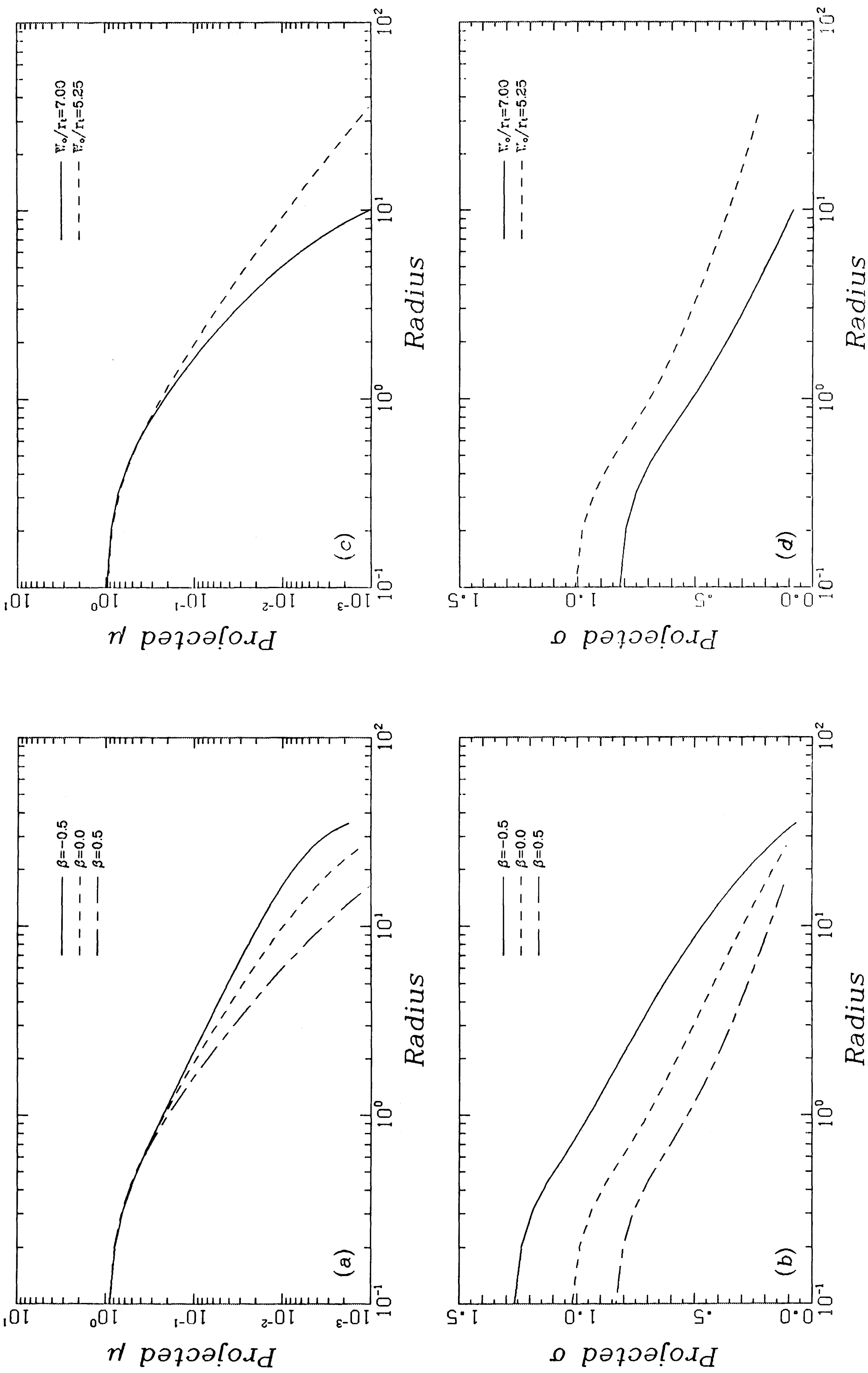

FIG. 3. Properties of power-law models. (a) Projected surface-density profile showing the effects of varying the exponent β. (b) Projected velocity-dispersion profile for (a). (c) Same as (a), but showing the effect of varying W_0/r_t. (d) Same as (c), but for the velocity-dispersion profile.

tropic model rising slightly above at larger radii. However, the anisotropic model is actually infinite in size. This illustrates a characteristic property of King-Michie models: there is a minimum value of r_t below which the models becomes infinite in size and mass. Numerically it is found that this minimum r_t is about 15% of the limiting radius of the corresponding isotropic model. To generate models with finite size and smaller r_t requires that a different form for the energy-distribution function be used. In a moment we shall see that a power-law distribution meets the necessary requirements.

Finally, in Fig. 2(d) we show the effects of a central massive object (using the "filled center" case of Sec. V f) on the core surface-density profile. Three values of M_i (0, 0.2, and 0.4) are plotted (again, $W_0 = 8$); for comparison, the total dimensionless mass inside $r = 1$ is 2.2. These curves have been shifted vertically slightly to align the profiles at large radii. As expected, the density is enhanced at small radii with a central mass present, but then it falls below the unperturbed profile before joining on smoothly at $r \simeq 6$. It is thus seen that a modest central mass can distort the profile significantly, making possible a method for estimating the masses of central galaxies in clusters.

b) $f_2 = E^\beta \exp(-J^2/2J_0{}^2)$ *(Power Law)*

The scaling parameters are taken such that ρ_0 is the central density. There is no longer a natural scale velocity, and changing the central potential W_0 produces rescaled versions of the same model. A dimensionless mod-

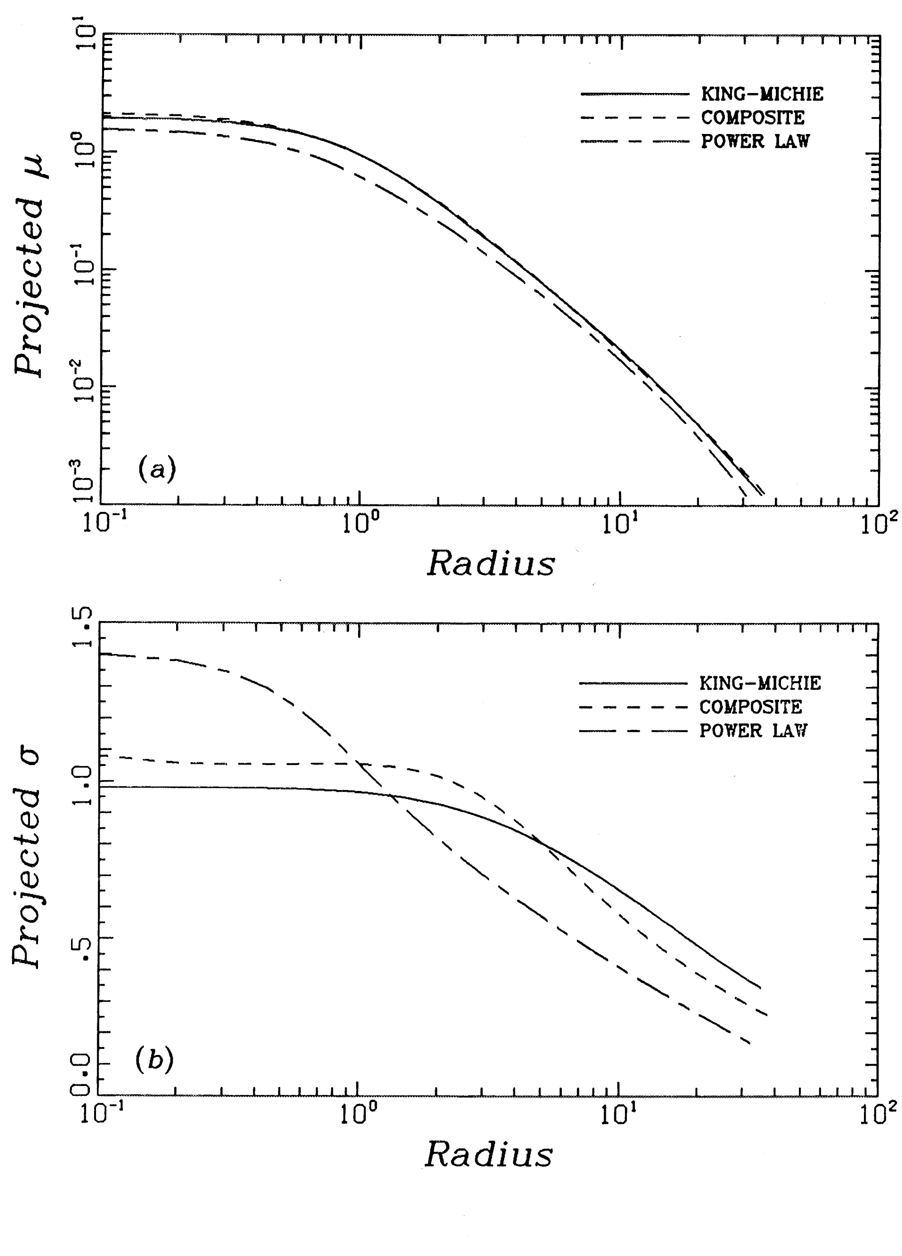

FIG. 4. Surface-density and velocity-dispersion profiles for three dynamical models that have nearly identical surface-density profiles.

el is specified by the power-law exponent β and the quantity W_0/r_t.

These models are of greatest interest for small values of r_t, i.e., large anistropy. In Figs. 3(a) and 3(b) we show the surface density and velocity dispersion profiles for three models that illustrate the effect of varying the parameter β. All three models have the same limiting radius and a value of W_0/r_t near 6. Figures 3(c) and 3(d) show the effect of keeping β fixed but varying W_0/r_t.

Several features of these models are evident:

(1) There is a core region similar in shape to that of King models.

(2) Beyond the core is a halo with a nearly power-law shape. Asymptotically we would expect $\rho \propto r^{-(\beta+5/2)}$ for models infinite in extent.

(3) There is a sharp cutoff at the limiting radius, models with smaller β having a sharper cutoff.

(4) The overall size of a model is determined primarily by the parameter W_0/r_t; larger values yield larger clusters.

(5) The velocity dispersion drops rapidly from the center towards the cluster edge.

It is this last feature that is characteristic of models with significant anisotropy. For these power-law models the anisotropy is quite pronounced: at large r the tangential dispersion falls to 0 like $\sigma_t \propto 1/r$.

The importance of having dynamical information for a cluster is vividly illustrated in Fig. 4. Here we plot three models that have virtually identical surface-density profiles (at least in the range of radii where cluster

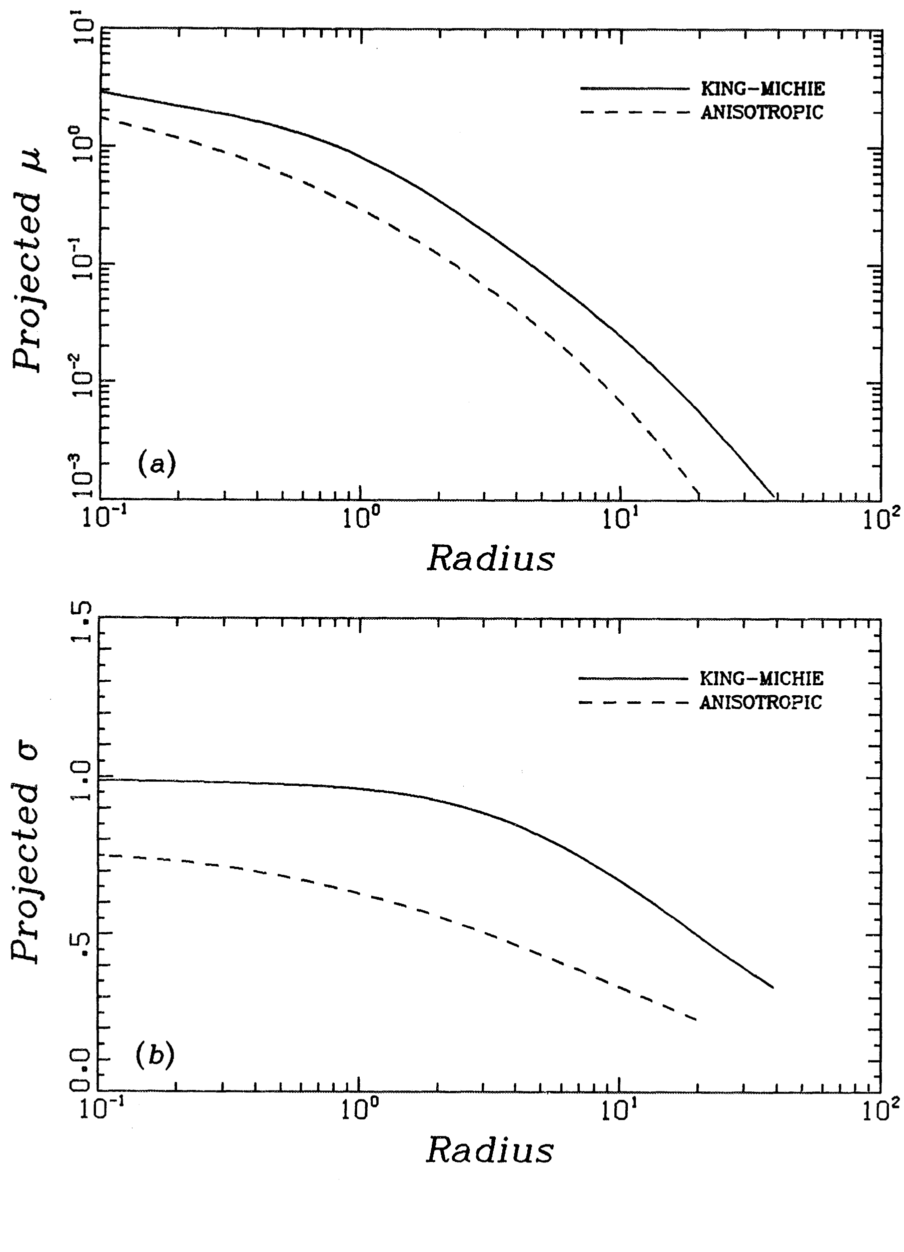

FIG. 5. Same as Fig. 4 but comparing a King-Michie model with a central massive object to a constant-anisotropy model (labeled "ANISOTROPIC").

profiles can be determined) and yet have markedly different internal dynamics. The first is a power-law model with $\beta = 0.5$, $W_0 = 5.88$, $r_t = 0.98$. The second is a King-Michie model with $W_0 = 8.5$, $r_t = 13$, and a central mass $M_i = 0.04$ (we have used the "empty center" distribution for this last case; i.e., $f = 0$ for $E > W_0$). The third is a composite model with a distribution function of the form $f = \alpha f_1 + (1-\alpha) f_2$, where f_1 and f_2 are the King-Michie and power-law distributions, respectively. The parameters are taken to be $W_0 = 8.5$, $r_t = 5$, $M_i = 0.04$, and α is selected such that the King-Michie distribution contributes 95% of the total density at $r = 0$. This composite model illustrates how one can form dynamical models with the transition radius r_t intermediate in value between the very small values of the power-law models and the relatively large values of the King-Michie models. The surface-density profiles in Fig. 4 are so similar that all would give equally good fits to a cluster profile. It is only with velocity dispersions that one can differentiate the three models.

c) $f_3 = (\exp E - 1) J^{-\gamma}$ (Constant Anisotropy)

The scaling parameter σ is taken to be the characteristic velocity dispersion in the distribution function. For $\gamma > 0$, these models have infinite central space density ($\rho \propto r^{-\gamma}$), and so there is no natural scale density. We therefore arbitrarily select a radius at which $\rho = 1$ (changing this radius produces rescaled versions of the same model). A dimensionless model is specified by the parameters W_0 and γ. In the Appendix it is shown that the ratio of tangential to radial velocity dispersions is everywhere given by $\langle h^2 \rangle / \langle v^2 \rangle = 2 - \gamma$.

In Fig. 5 we show one typical model and compare it with a King-Michie model. The King-Michie model has parameters $W_0 = 8.5$, $r_t = 15$, $M_i = 0.2$, and the anisotropic model has $W_0 = 3.6$, $\gamma = 1$. In general, these constant-anisotropy models are rather similar to King-Michie models with a central massive object, although the profiles for the former tend to be somewhat smoother. These similarities suggest that anisotropy in the scale-free form that we have used will be very difficult to distinguish observationally, even with full dynamical information.

Finally, we digress slightly to point out that the continuous rise of surface density at small radii (owing to the infinite central density) is also characteristic of a de Vaucouleurs law, $\log \mu = \log \mu_0 - 3.33 (r/r_e)^{1/4}$. Depending on the values of W_0 and γ that are picked, the constant-anisotropy models provide a reasonable approximation to a de Vaucouleurs law over a surprisingly large range. For example, taking $W_0 = 4.5$, $\gamma = 1$ gives a good match over nearly three decades in radius $[-2 < \log(r/r_e) < 1]$. Whether this coincidence has any relevance to the dynamics of elliptical galaxies remains to be seen.

d) $f_4 = E^{\beta} J^{-\gamma}$ (Scale-free)

For $\beta > 2$, E^{β} becomes a reasonable approximation to $\exp E - 1$, and models with this distribution function look rather similar to the constant-anisotropy models of Sec. IV c. Otherwise, this pure scale-free distribution produces models that are rather truncated in appearance, and they will not be pursued further.

VII. COMPARISON WITH COMA

a) Fitting Procedure

The fitting procedure is quite straightforward. Any dimensionless model is specified by parameters such as W_0, r_t, M_i, β, etc. Given a dimensionless model, we can then adjust the dimensional parameters σ, μ_0, and r_s to match the observed cluster profiles. The central density ρ_0 cannot be measured directly but is inferred from r_s and σ via Eq. (3).

The observed quantities consist of the two surface-density profiles in Table II and the velocity-dispersion profile in Table III. The two surface-density profiles have been merged into one composite profile by multiplying the radial-velocity-selected sample by a factor of 2.57, which is simply the ratio of the total number of objects within 29′ for each sample. With about 20 objects per data point, a standard least-squares fit is possible. We take as observables $\ln \mu$ and $\ln \sigma$. Having judiciously binned the data to give approximately equal numbers of objects per data point, all observations are given equal weight in the fit.

Because of its higher accuracy, we have fit only to the surface-density profile, and then used the velocity-dispersion profile only to determine if the quality of the dynamical fit is acceptable.

b) Results

As we have anticipated in Sec. VI, there is no unique best-fitting model. Models with rather different characteristics can be difficult to distinguish observationally, particularly since the density- and velocity-dispersion profiles for a cluster are limited by the finite number of galaxies in a cluster. In Table VI we gather together the parameters for the best-fitting models for each type of distribution function that we have investigated. Here we comment briefly on the fits.

1) King-Michie Distribution

An isotropic King model fits the cluster observations surprisingly well, in agreement with the conclusions reached by RPKK. Allowing for anisotropy in the distribution function (i.e., making r_t finite) does not noticeably affect the quality of the fit, the reason being that even for a maximally anisotropic model (where the cluster becomes infinite in size), the transition radius is so large ($r_t \geqslant 10$) that the models are virtually unchanged in the inner regions that correspond to the observable cluster. Allowing for a central massive object does improve the fit in the core region somewhat. Quintana (1979) has previously noted difficulties with fitting the inner core,

TABLE VI. Results of fits to Coma.

Distribution function	Dimensionless parameters	r_s (′)	σ (km s^{-1})	χ^2 μ[a]	σ[b]
King-Michie	$W_0 = 8.6$, $r_t = \infty$, $M_i = 0$	8.5	1091	7.7	15.1
	$W_0 = 8.0$, $r_t = \infty$, $M_i = 0.2$	10.0	1110	7.2	15.1
Power law	$W_0 = 4$,[c] $r_t = 0.662$, $\beta = 0.5$	11.0	1643	6.9	42.0
Constant anisotropy	$W_0 = 6.4$, $\gamma = 0.5$	5.5[d]	1272	7.0	14.1
	$W_0 = 3.9$, $\gamma = 1.0$	2.55[d]	1728	7.4	15.0

[a] Surface-density profile; 14 degrees of freedom.
[b] Velocity-dispersion profile; 14 degrees of freedom.
[c] W_0 fixed arbitrarily.
[d] For dimensionless density arbitrarily scaled to $\rho = 1$ at $r = 0.1$.

in that the observed central density rises somewhat above that predicted by an isothermal sphere. The mass of this central object M_i is highly correlated with W_0 and r_s, and so is not well determined. In Table VI we give the best-fitting parameters for the two cases $M_i = 0$ and 0.2 (again, using the "filled center" distribution); this latter value can be regarded as an upper limit on M_i since larger values rapidly degrade the fit. In Fig. 6 we plot the observed profiles along with the fit for the $M_i = 0.2$ case.

2) Power-law Distribution

As expected, the parameters for this distribution can be adjusted to give an excellent match to the surface-density profile, but the velocity-dispersion profile is all wrong. We have also tried fitting the composite models of Sec. VI b (summing a King-Michie and power-law distribution) to determine if intermediate values of r_t were possible. Such models, however, also gave poor fits to the dynamics, the problem being, as illustrated in Fig. 4, that the predicted velocity-dispersion profile is flat for $r < r_t$ with a steep drop outside this radius, whereas the observed profile declines more gradually with radius.

3) Constant-anisotropy Distribution

These models give good fits to both the density- and velocity-dispersion profiles. The parameter γ is not well constrained, and in Table VI we list models for the cases $\gamma = 0.5$ and 1. Because these models have infinite central density, there is no need to consider the addition of a central massive object.

c) Discussion

The results of the previous section can be summarized by saying that the best fits to Coma are achieved by models with constant anisotropy (including the case of pure isotropy); models for which the galaxy motions are isotropic in the core and radial in the halo can be ruled out by the dynamical data.

Having made this statement we issue two caveats. First, we have clearly not explored all possible forms for the distribution function $f(E,J)$ and thus cannot claim to have found *the* correct one. In view of the limited statistics in determining the cluster profile necessarily set by the finite number of galaxies in the cluster, it is not clear if pursuing any further variations to our models would be fruitful. Second, all of our models extend to much larger radii than are reasonable for Coma. For example, the isotropic King model with $W_0 = 8$ has a limiting radius of 68 core radii or $\sim 11°$ on the sky. A galaxy infalling from such a radius would not have reached the cluster center during the age of the universe. Very likely the outskirts of Coma are not in equilibrium and so the extension of our static models to these regions is not justified.

The conclusions regarding the dynamics of Coma that we infer from our dynamical models are in conflict with the results of n-body simulations (Peebles 1970; Gott 1975; White 1976). These simulations, which follow the collapse of systems that are intially spherically symmetric, produce clusters that are very much like the anisotropic King-Michie models. Our results suggest that the galaxies in Coma at large radii have considerably more kinetic energy in the tangential direction than these simulations produce. We also find that the density profiles generated by these simulations do not agree in detail with that observed for Coma. It is possible that the use of more realistic initial conditions for the density perturbations used in the collapse calculations would lead to clusters which better resemble Coma, but such matters are best left to the n-body specialists.

VIII. ADDITIONAL TOPICS

In this section we discuss a diverse range of topics regarding the structure and dynamics of Coma.

a) Core Radius

Traditionally, the core radius of a cluster is defined to be the radius at which the projected surface density of galaxies falls to one-half of its central value. In practice it is determined by scaling some convenient analytic law to fit the observed density profile. While the core radius

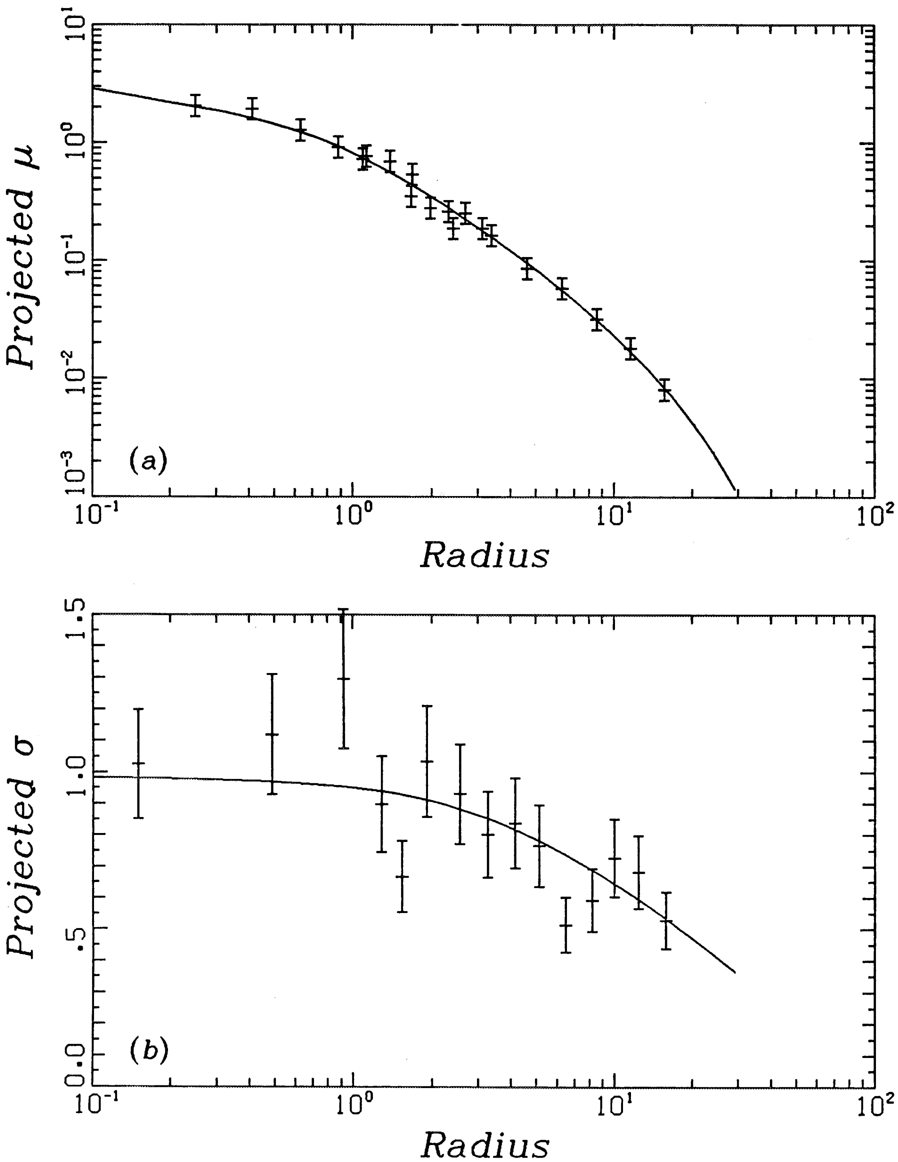

FIG. 6. Comparison of observed surface-density and velocity-dispersion profiles with predictions for a King-Michie model ($W_0 = 8$, $M_i = 0.15$, $r_t = \infty$). Radius is in units of $r_s = 8.5'$.

is an oft-quoted parameter used to describe the galaxy distribution in a cluster, it is not generally recognized how poorly determined this quantity can be. The specific density law used, the method by which one bins the data, the background density used, and the radius to which a profile is measured all affect the value one gets for a core radius. We find that after allowing for all these factors the core radius one derives can vary by typically 20%, even when the set of galaxies used is unchanged. When allowance is made for errors in selecting the cluster center and choosing a magnitude-limited sample, it is not surprising that different investigators find different core radii for the same clusters. The maximum-likelihood method of Sarazin (1980) avoids some of these problems and, provided one keeps the background correction fixed, has much to commend for itself.

Using King models, we find a core radius for Coma of 8.5′–10′ (depending on the value of W_0 used), or 340–400 h_{50}^{-1} kpc, where h_{50} is (H_0/50 km s^{-1} Mpc^{-1}) and H_0 is the Hubble constant. This value is significantly larger than the 6′ found by RPKK and Bahcall (1973). The discrepancy with RPKK is due in part to the fact that they fit a more extended King model ($W_0 = 9.33$), which leads to a smaller core radius; in addition their data set is not likely to be as good as that used here. The discrepancy with Bahcall appears to be mainly a differencee between her surface-density profile and ours; if we fit her profile using our procedures we also derive a small core radius. The source of the discrepancy is not obvious, but since her number counts rely on eyeball estimates of galaxy magnitudes, it is possible that she has a systematic variation in limiting magnitude with radius that will lead to an erroneous profile. Dressler (1978) also finds that Bahcall's core radii for other clusters are systematically low.

b) Central Massive Object

In Table VI we have listed the details for one model that contains a central massive object. In physical units this mass corresponds to $1.5 \times 10^{13}\ h_{50}^{-1}\ M_{\odot}$. As we have mentioned, this mass is not well determined and should be regarded as an upper limit. It should also be pointed out that this figure refers only to the mass within $0.1 r_s$, or 40 kpc of the cluster center. Since the mass distribution in our models is continuous, it is not obvious how much mass should be attributed to a single central galaxy and how much is contained in other galaxies or a "dark" component. Nevertheless, it is quite clear that a mass $\sim 10^{14} M_{\odot}$ for either NGC 4874 or NGC 4889, as has been suggested by Wolf and Bahcall (1972) and Valtonen and Byrd (1979), is quite implausible. Dressler (1979) presents a more detailed treatment of the dynamics of a cD galaxy in the potential well of a cluster.

c) Total Mass and M/L Ratio

The total mass in Coma as presented by our models turns out to be quite insensitive to the specific model used. We find the total projected mass inside a radius of 3° to be $2.9 \times 10^{15}\ h_{50}^{-1} M_{\odot}$. For the moment, we do not attempt to extrapolate beyond this radius.

The total luminosity is computed as follows. Godwin and Peach (1977) find that the cumulative luminosity function in the central regions of Coma can be fit with a double power-law function:

$$\log N\ (\leqslant m) = \alpha_1 + \beta_1 m, \quad m < m_*,$$

$$\log N\ (\leqslant m) = \alpha_2 + \beta_2 m, \quad m > m_*,$$

with $m_* = 14.92$, $\beta_1 = 0.64$, $\beta_2 = 0.25$; α_1 and α_2 are normalization constants. Integrating, we find the total luminosity to be

$$L = 4.33 L_* N_*,$$

where L_* is the luminosity of a galaxy at m_*, and N_* is the total number of galaxies brighter than L_*. Converting to Zwicky magnitudes, we find $m_* = 15.86$, and $L_* = 1.3 \times 10^{10}\ h_{50}^{-2}\ L_{\odot}$. Inside $R = 3°$, we find 220 galaxies brighter than $m_p = 15.7$ that are cluster members. Extrapolating to m_*, we estimate that $N_* = 279$, and hence the total blue luminosity is $L_B = 1.6 \times 10^{13}\ h_{50}^{-2}\ L_{\odot}$. In the V band we would predict $L_V = 2.1 \times 10^{13} h_{50}^{-2} L_{\odot}$, which is close to the value derived by Abell (1977). Then the ratio of total mass to blue light is

$$M/L_B = 181 h_{50}^{-1}.$$

Note that the most uncertain quantity is the total luminosity, which requires a large but uncertain correction for fainter galaxies. This value of M/L is in reasonable agreement with that of other workers (e.g., RPKK).

d) Cosmological Infall and the Cluster "Edge"

In the standard picture of cluster formation (Gunn and Gott 1972), outside of the virialized cluster regions there lies material that is dynamically bound to a cluster but that has not yet had time to collapse. A convenient definition for the edge of a cluster is that shell that has been decelerated from the Hubble flow and is just now turning around. Gunn and Gott (1972) have shown that this radius is

$$R_{v=0} = \left(\frac{8GMt_0^2}{\pi^2}\right)^{1/3},$$

where M is the total mass within this radius and t_0 is the age of the universe. The value for the zero-velocity radius will depend somewhat on q_0; for example, taking $M = 3 \times 10^{15}\ M_{\odot}$ and $q_0 = 0.5$, we get

$$R_{v=0} = 12.3 h_{50}^{-1}\ \text{Mpc, or } \theta_{v=0} = 5\overset{\circ}{.}2.$$

Note that the angular radius is independent of H_0. For q_0 ranging between 0 and 1, this radius varies from 4.7° to 6.8°. If one carefully studied the velocity field around Coma, conceivably one could determine this angle directly and hence estimate q_0.

As we have noted previously, Tifft and Gregory (1976) find that Coma is not distinguishable from the surrounding supercluster beyond a radius of 3°. When allowance is made for projection effects, we see that the cluster indeed terminates about where we would expect it to.

e) Velocity Cutoff

A prediction of our static equilibrium models is that at each point in a cluster there should be no galaxies with a velocity that exceeds the local escape velocity. "Escape" is not a well-defined term for a cluster that is not isolated from its surroundings, but having established a formal edge to a cluster in the previous section, we now defined escape velocity as being the velocity necessary to reach a radius of $\sim 5°$. The actual value that we compute for the escape velocity depends very little on the dynamical model used. In Fig. 1, the lines we have drawn to separate cluster members from field galaxies are, in fact, precisely the local escape velocity at each radius. It is gratifying to find that the cluster members are indeed confined within the envelope so drawn, with only a few questionable objects.

f) Distribution of "Dark Matter"

A prime question (of course) is the nature and distribution of the dark material that presumably binds clusters. Up to this point we have implicity assumed that such dark matter is distributed like the galaxies and now we consider the implications of relaxing this assumption.

First we note that variations in the distribution of dark matter are reflected only insofar as the galaxies (now considered to be test particles) respond to the resulting potential so generated. Since the potential will smooth out any small-scale variations in the density of dark matter, only large-scale variations in the distribution will be detected. Qualitatively we can estimate how the density- and velocity-dispersion profiles will be altered simply on the basis of hydrostatic equilibrium. If the dark matter is more concentrated than the galaxies, then we would expect the velocity dispersion of the galaxies σ_g to rise in the cluster center. Conversely, if the dark matter is more extended, then σ_g should not fall as rapidly at large radii than it would otherwise.

The only quantitative calculations that we have done are for the case that the dark matter is distributed like an isothermal sphere with a core radius the same as that for the galaxies. The galaxies are now nothing more than test particles distributed within this potential well. After a little experimentation it was found that a King-Michie distribution with parameters $W_0 = 10$, $r_t = 18$, and a core radius $r_c = 9'$ could once again make a good fit to the surface-density profile (being, in fact, indistinguishable from the curve in Fig. 6). However, the velocity-dispersion profile, as expected, does not fill as well (χ^2 increases from 15 to 18). While one would be reluctant to conclude definitively that the galaxies and gravitating matter are distributed identically, it is certainly true that there is no observational evidence to the contrary.

g) Morphological Segregation

We have shown in Sec. IV c that galaxies in Coma are segregated by morphological type, and have provided a quantitative measure of the degree of segregation for those galaxies inside $R = 1°$. We now ask if it is possible to incorporate the three different types of objects into our models which heretofore have contained only a single class of objects.

For theoretical models we restrict ourselves to the isotropic King model with $W_0 = 8$ and no central mass. We have tried two methods of simulating segregation within the cluster.

(1) Ignoring the problems of self-consistency, galaxies of each morphological type are treated as test particles in the potential well of the cluster with a central velocity dispersion different from that of the cluster model. Thus, e.g., spirals will have a higher velocity dispersion and hence a more extended distribution than ellipticals.

(2) The total distribution function $f(E, J)$ is carved up into three fractions representing each morphological class:

$$f_{\text{total}} = f_{\text{Sp}} + f_{\text{S0}} + f_{\text{E}}.$$

To allow for segregation in the simplest case we partition on the basis of energy alone:

$$f_i = (\alpha_i - \beta_i E) f_{\text{total}},$$

where α_i, β_i are constants adjusted so that (i) $\Sigma f_i = f_{\text{total}}$; (ii) the number fraction and median radius of class i are approximately reproduced.

Both methods yield virtually identical results, which are summarized in Table IV. Basically, we can reproduce the segregation (i.e., median radius) without difficulty, but the range in velocity dispersion for the different morphological classes is computed to be only half that which is observed. This result is rather marginal since the measured dispersions have statistical errors of $\sim 10\%$, but, if true, indicates that morphological segregation is characterized by more than simply differences in energy distribution. This result is, of course, of great interest to the problems of galaxy formation and understanding how morphological segregation originally arises.

h) X-ray Emission

Clusters of galaxies like Coma have strong x-ray emission from a hot intracluster medium that sits within the potential well of the cluster. If this medium is in hydrostatic equilibrium, it can, in principle, provide a powerful probe for investigating the potential distribution in a cluster, since (i) one does not have to worry about anisotropic pressure distributions, and (ii) the x-ray profile is not limited by counting statistics as is the galaxy profile. In practice, the fundamental limitation is that current x-ray imaging detectors are unable to map the temperature profile of these high-temperature sources, so any firm conclusions must rest upon one's assumptions about any temperature variation in the intracluster medium. Mushotzky *et al.* (1978) comment that for well-observed clusters, their x-ray spectra are inconsistent with a single-temperature medium, although they cannot say anything about what form the temperature variation in a cluster should be.

To demonstrate how ambiguous this lack of temperature information can be, we have calculated the x-ray emissivity from a gas resting in the potential well of the Coma cluster and tried to establish if the presence of a central massive object in the center of Coma as inferred in Sec. VII is plausible.

Given the potential within a cluster it is quite straightforward to compute the gas density. For hydrostatic equilibrium to hold we have

$$\frac{dP}{dr} = -\rho \nabla \Phi,$$

where P is the gas pressure, ρ the density, and Φ the potential. Following Bahcall and Sarazin (1977) we consider two cases for the temperature distribution:

(i) Isothermal, $T = T_0, \rho = \rho_0 e^{\beta W}$,

(ii) Polytropic, $T = T_0(\rho_0/\rho)^{\gamma - 1}$,

$$\rho = \rho_0 \left(\frac{\gamma - 1}{\gamma} \beta (W - W_0) + 1 \right)^{1/\gamma - 1},$$

where γ is the polytropic index, $\beta = \mu\sigma^2/kT_0$, W is the dimensionless potential, and T_0, ρ_0 are the central temperature and density, respectively. μ is the mean molecular weight of the gas, and σ is the characteristic galaxy

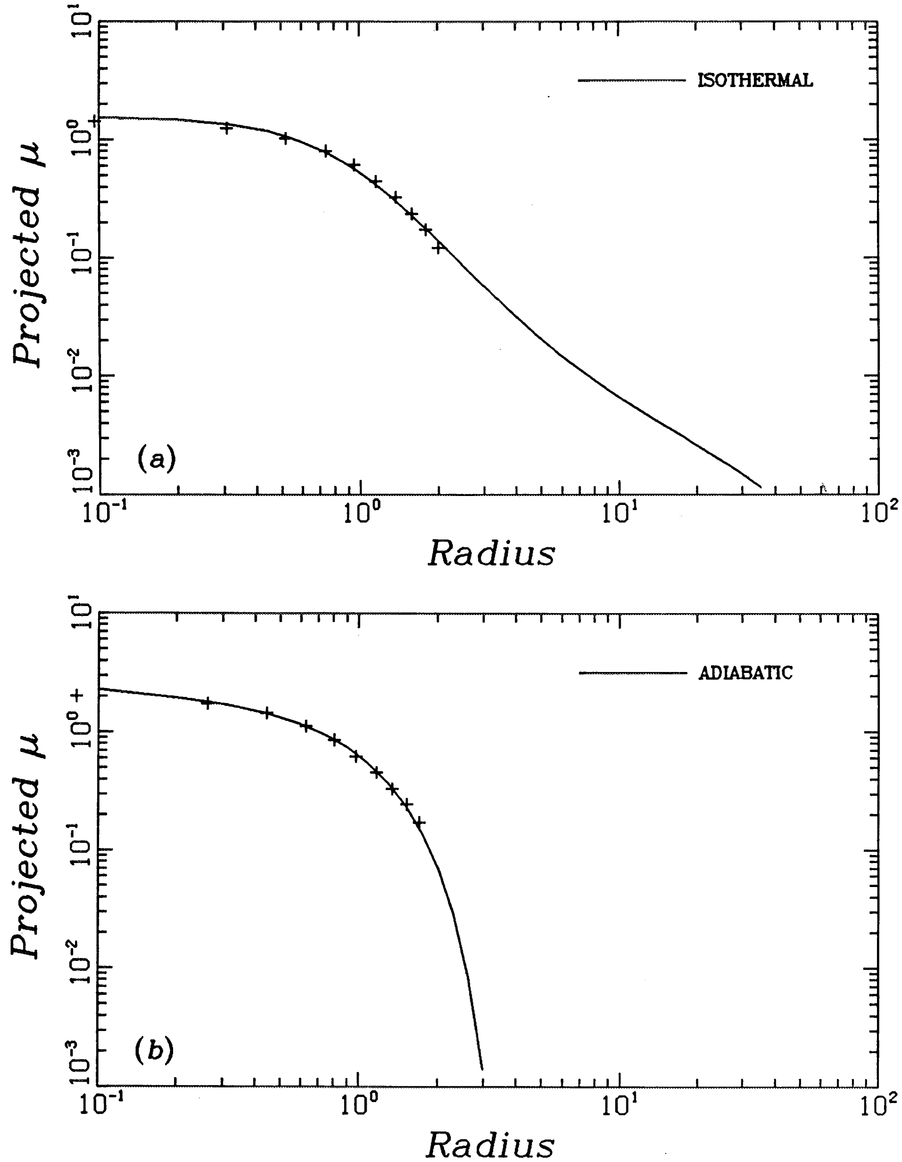

FIG. 7. Predicted x-ray intensity profile for Coma. (a) Cluster: King model ($W_0 = 8.5$, $M_i = 0$, $r_t = \infty$, $r_s = 8.5'$). Gas: isothermal distribution ($\beta = 0.67$). (b) Cluster: King model ($W_0 = 8.0$, $M_i = 0.20$, $r_t = \infty$, $r_s = 10'$). Gas: adiabatic distribution ($\beta = 0.61$, $\gamma = 5/3$).

velocity dispersion. We compute the emissivity at an energy of 3 keV (which is characteristic of the *Einstein* observatory detectors), using formulas from Gould (1980).

For the cluster potential, we use the two King-Michie models from Table VI, one with a central mass and the other without. For the emissivity profile of Coma, we use the *Einstein* observations of Abramopolous, Chanan, and Ku (1981).

In Fig. 7 we show two equally acceptable fits to the observed profile:

(i) Isothermal gas, no central mass;

$\beta = 0.67$,

(ii) Adiabatic gas, central mass;

$\beta = 0.60$, $\gamma = 5/3$.

If the gas were everywhere isothermal, we could rule out the presence of a massive object in the center of Coma; the density and emissivity would rise much too rapidly towards the center. However, if the temperature rises in the center, as with the adiabatic models, the gas does not respond as fast to the potential of the central mass and the emissivity profile remains flatter. The rapid drop in emissivity of the adiabatic profile near $r \sim 2r_s$ could, of course, be rectified by fixing the gas temperature to a constant value beyond this radius. Even if the temperature profile were known, Abramopolous *et al.* have demonstrated that composition gradients in the hot medium (such as might arise from heavy elements preferentially "settling out" as they must if in equilibrium) can further alter the x-ray structure. In summary, without detailed temperature (and possibly spectralline) information, x-ray profiles cannot place strong constraints on the core structure of Coma.

IX. CONCLUSIONS

Our main conclusion in this paper is that the dynamics of the Coma cluster can be well represented by simple analytical models. Although observationally one cannot select any single best-fitting model, we can nevertheless place certain constraints on the dynamics of Coma. Thus, e.g., we have shown that the galaxy orbits in Coma cannot be primarily radial, or we would observe a much steeper gradient in velocity dispersion from center to edge than is observed. Even at large radii, a significant fraction of the kinetic energy must be in the tangential direction. Our models allow for the existence of a modest central mass in the core of Coma ($\sim 10^{13} M_\odot$),but definitely rule out the existence of a supermassive object ($> 10^{14} M_\odot$), at least on a scale much smaller than the cluster core radius.

We have emphasized the necessity for having radial velocities in studying cluster dynamics, particularly in the outlying regions. They serve not only to define the velocity-dispersion profile but also to separate cluster members from field galaxies. We have also shown that the surface-density profile alone is not enough to determine a cluster's dynamics: it is possible for two equally plausible models with completely different internal dynamics nevertheless to have virtually indistinguishable density profiles, at least in the range of densities covered by cluster observations.

In closing, we point out that Coma is quite atypical among clusters in its richness, compactness, and degree of symmetry. The more numerous irregular clusters are not likely to have reached a state of dynamical equilibrium and hence are probably not amenable to the type of analysis which we have applied to Coma. In our next paper we shall investigate the Perseus cluster which, although it is not been as well studied as Coma, is equally as rich and is, in some ways more interesting.

We wish to thank M. Davis and M. Lecar for several valuable discussions.

APPENDIX: EVALUATION OF THE INTEGRALS OF THE DISTRIBUTION FUNCTION

The integrals in Eq. (4a)–4(c) are evaluated here for distribution functions in Eq. (2a)–(2d). For simplicity we defined the following two functions:

$$D^{-}(X) = e^{x^2}\int_0^x e^{-t^2}\,dt,$$
$$D^{+}(X) = e^{-x^2}\int_0^x e^{t^2}\,dt, \qquad \text{(A1)}$$

which are variants of the error function and Dawson's integral, respectively (Abramowitz and Stegun 1964).

a) $f_1 = (\exp E - 1)[\exp(-J^2/2J_0{}^2)]$

Letting $J_0 = r_t$ we have

$$\rho = 4\pi \int_0^{(2W)^{1/2}} dv \int_0^{(2W - v^2)^{1/2}} \times[\exp(W - \tfrac{1}{2}v^2 - \tfrac{1}{2}h^2) - 1] \times \exp(-h^2 r^2/2r_t{}^2) h\,dh, \qquad \text{(A2)}$$

etc. Then ρ is an explicit function of W and $\chi = r/r_t$. We get

$$\rho = 4\pi 2^{1/2}[b_1 D^{-1}(W^{1/2}) + (b_2 - b_1) b_2{}^{1/2} D^{+}(W^{1/2}\chi) - b_2 W^{1/2}], \qquad \text{(A3a)}$$

$$\rho\langle v^2\rangle = 4\pi 2^{1/2}[b_1 D^{-1}(W^{1/2}) - (b_1 - b_2) b_2{}^{3/2} D^{+}(W^{1/2}\chi) + (b_2{}^2 - b_1 b_2 - b_1) W^{1/2} - 2/3 b_2 W^{3/2}], \qquad \text{(A3b)}$$

$$\rho\langle h^2\rangle = 8\pi 2^{1/2}\{b_1{}^2 D^{-}(W^{1/2}) + [b_2{}^2 - b_1{}^2 + (b_2 - b_1)(W + \tfrac{1}{2}b_2)] b_2{}^{1/2} D^{+}(W^{1/2}\chi) - [b_2 + \tfrac{1}{2}(b_2 - b_1)] b_2 W^{1/2}\}, \qquad \text{(A3c)}$$

where we have let $b_1 = 1/(1 + \chi^2)$ and $b_2 = 1/\chi^2$. In the limit $r_t \rightarrow \infty$, these equations reduce to

$$\rho = 4\pi 2^{1/2}[D^{-}(W)^{1/2} - 2/3 W^{3/2} - W^{1/2}], \qquad \text{(A4a)}$$

$$\rho\langle v^2\rangle = 4\pi 2^{1/2}[D^{-}(W^{1/2}) - 4/15 W^{5/2} - 2/3 W^{3/2} - W^{1/2}], \qquad \text{(A4b)}$$

$$\rho\langle h^2\rangle = 2\rho\langle v^2\rangle. \qquad \text{(A4c)}$$

These functions must all be normalized such that $\rho = 1$ at $r = 0$.

b) $f_2 = E^\beta \exp(-J^2/2J_0{}^2)$

We have

$$\rho = 4\pi \int_0^{(2W)^{1/2}} dv \int_0^{(2W - v^2)^{1/2}} (W - \tfrac{1}{2}h^2 - \tfrac{1}{2}v^2)^\beta \times \exp(-h^2 r^2/2r_t^2) h\,dh,$$

etc. These integrals can be evaluated explicitly only for integer and half-integer values of β. A few cases are shown below, where again $\chi = r/r_t$.

$\beta = -\frac{1}{2}$:

$$\rho = \frac{4\pi^2}{2^{1/2}\chi^2}[1 - \exp(-W\chi^2)], \qquad \text{(A5a)}$$

$$\rho\langle v^2\rangle = \frac{4\pi^2}{2^{1/2}\chi^4}[W\chi^2 - 1 + \exp(-W\chi^2)], \qquad \text{(A5b)}$$

$$\rho\langle h^2\rangle = 2W\rho - 2\rho\langle v^2\rangle; \qquad \text{(A5c)}$$

$\beta = 0$:

$$\rho = \frac{4\pi 2^{1/2}}{\chi^3}[W\chi^2 - D^{+}(W^{1/2}\chi)], \qquad \text{(A6a)}$$

$$\rho\langle v^2\rangle = \frac{4\pi 2^{1/2}}{\chi^5}[2/3(W\chi^2)^{3/2} - (W\chi^2)^{1/2} + D^{+}(W^{1/2}\chi)], \qquad \text{(A6b)}$$

$$\rho\langle h^2\rangle = 2W\rho - 3\rho\langle v^2\rangle; \qquad \text{(A6c)}$$

$\beta=\frac{1}{2}$:

$$\rho=\frac{2\pi^2}{2^{1/2}\chi^4}[W\chi^2-1+\exp(-W\chi^2)], \tag{A7a}$$

$$\rho\langle v^2\rangle=\frac{2\pi^2}{2^{1/2}\chi^6}[\tfrac{1}{2}(W\chi^2)^2-W\chi^2+1-\exp(-W\chi^2)], \tag{A7b}$$

$$\rho\langle h^2\rangle=2W\rho-4\rho\langle v^2\rangle. \tag{A7c}$$

In the limit that $r_t\rightarrow\infty$ we get

$\beta=-\frac{1}{2}$:

$$\rho=\frac{4\pi^2}{2^{1/2}}W, \tag{A8a}$$

$$\rho\langle v^2\rangle=\rho W/2, \tag{A8b}$$

$$\rho\langle h^2\rangle=2\rho\langle v^2\rangle; \tag{A8c}$$

$\beta=0$:

$$\rho=\frac{8\pi 2^{1/2}}{3}W^{3/2}, \tag{A9a}$$

$$\rho\langle v^2\rangle=\rho W/2.5, \tag{A9b}$$

$$\rho\langle h^2\rangle=2\rho\langle v^2\rangle; \tag{A9c}$$

$\beta=\frac{1}{2}$:

$$\rho=\frac{\pi^2}{2^{1/2}}W^2, \tag{A10a}$$

$$\rho\langle v^2\rangle=\rho W/3, \tag{A10b}$$

$$\rho\langle h^2\rangle=2\rho\langle v^2\rangle. \tag{A10c}$$

c) $f_3=(\exp E-1)J^{-\gamma}$

These integrals are most easily evaluated by putting them in the form of Eq. (5b):

$$\rho=4\pi\int_0^W dE\int_0^{r[2(W-E)]^{1/2}}\times\frac{(\exp E-1)J\,dJ}{J^\gamma r^2[2(W-E-J^2/2r^2)]^{1/2}},$$

etc. Letting $\delta=(1-\gamma)/2$, we get

$$\rho=4\pi 2^{\delta-1}\frac{\Gamma(\delta+\frac{1}{2})\Gamma(\frac{1}{2})}{\Gamma(\delta+1)r^\gamma}\int_0^W(e^E-1)(W-E)^\delta\,dE.$$

$\Gamma(x)$ is the standard gamma function.

Similar equations are derived for $\rho\langle v^2\rangle$ and $\rho\langle h^2\rangle$ by noting that $v^2=2(W-E-J^2/2r^2)$ and $h^2=J^2/r^2$. In general, these integrals must be evaluated numerically. For the special case $\gamma=1$ ($\delta=0$) we get

$$\rho=(e^W-W-1)/r, \tag{A11a}$$

$$\rho\langle v^2\rangle=\left(1-\frac{\frac{1}{2}W^2}{\exp W-W-1}\right)\rho, \tag{A11b}$$

$$\rho\langle h^2\rangle=\rho\langle v^2\rangle. \tag{A11c}$$

It can be shown for arbitrary γ that

$$\frac{\langle h^2\rangle}{\langle v^2\rangle}=2-\gamma.$$

Note that for isotropic orbits this ratio is 2 (the tangential direction has two degrees of freedom).

d) $f_4=E^\beta J^{-\gamma}$

Using Eq. (5b), the relevant integrals are readily evaluated:

$$\rho=4\pi\frac{2^{\delta-1}\Gamma(\delta+\frac{1}{2})\Gamma(\frac{1}{2})\Gamma(\beta+1)}{\Gamma(\beta+\delta+2)}\times W^{1+\beta+\delta}r^{-\gamma}, \tag{A12a}$$

$$\rho\langle v^2\rangle=\frac{\delta+1}{\beta+\delta+2}\rho W, \tag{A12b}$$

$$\rho\langle h^2\rangle=(2\delta+1)\rho\langle v^2\rangle, \tag{A12c}$$

where again, $\delta=(1-\gamma)/2$.

REFERENCES

Abell, G. O. (1977). Astrophys. J. **213**, 327.

Abramopolous, F., Chanan, G. A., and Ku, W. H. M. (1981). Astrophys. J. **248**, 429.

Abramowitz, M., and Stegun, I. A. (1964). *Handbook of Mathematical Functions* (National Bureau of Standards, Washington, D.C.).

Bahcall, N. A. (1973), Astrophys. J. **183**, 783.

Bahcall, J. N., and Sarazin, C. L. (1977). Astrophys. J. Lett. **213**, L 99.

Chandrasekhar, S. (1939). *An Introduction to the Study of Stellar Structure* (University of Chicago, Chicago), p. 96.

Chincarini, G., and Rood, H. J. (1972a). Astron. J. **77**, 4.

Chincarini, G., and Rood, H. J. (1972b). Astron. J. **77**, 448.

Chincarini, G., and Rood, H. J. (1976). Astrophys. J. **206**, 30.

de Vaucouleurs, G., de Vaucouleurs, A., and Corwin, H. G. (1976). *Second Reference Catalog of Bright Galaxies* (University of Texas, Austin).

Dressler, A. (1978). Astrophys. J. **226**, 55.

Dressler, A. (1979). Astrophys. J. **231**, 659.

Godwin, J. G., and Peach, J. V. (1977). Mon. Not. R. Astron. Soc. **181**, 323.

Gott, J. R. (1975). Astrophys. J. **201**, 296.

Gould, R. J. (1980). Astrophys. J. **238**, 1026.

Gregory, S. A. (1975a). Astrophys. J. **199**, 1.

Gregory, S. A. (1975b). Publ. Astron. Soc. Pac. **87**, 833.

Gregory, S. A., and Thompson, L. A. (1978). Astrophys. J. **222**, 784.

Gregory, S. A., and Tifft, W. G. (1976). Astrophys. J. **206**, 934.

Gunn, J. E. (1977). Astrophys. J. **218**, 592.

Gunn, J. E., and Gott, J. R. (1972). Astrophys. J. **176**, 1.

Gunn, J. E., and Griffin, R. F. (1979). Astron. J. **84**, 752.

King, I. R. (1966). Astron. J. **71**, 64.

Kintner, E. C. (1971). Astron. J. **76**, 409.

Lovasich, J. L., Mayall, N. U., Neyman, J., and Scott, E. L. (1961). In *Proceedings of the Fourth Berkeley Symposium on Mathematical Statistics and Probability*, edited by J. Neyman (University of California, Berkeley), p. 209.

Lynden-Bell, D. (1967). Mon. Not. R. Astron. Soc. **136**, 101.

Michie, R. W. (1963). Mon. Not. R. Astron. Soc. **125**, 127.

Mushotzky, R. F., Serlemitsos, P. J., Smith, B. W., Boldt, E. A., and Holt, S. S. (1978). Astrophys. J. **225**, 21.

Oemler, A. (1974). Astrophys. J. **194**, 1.

Peebles, P. J. E. (1970). Astron. J. **75**, 113.

Quintana, H. (1979). Astron. J. **84**, 15.

Rood, H. J. (1975). Astrophys. J. **201**, 551.

Rood, H. J., Page, T. L., Kintner, E. C., and King, I. R. (1972). Astrophys. J. **175**, 627 (RPKK).

Sarazin, C. L. (1980). Astrophys. J. **236**, 75.

Thompson, L. A., and Gregory, S. A. (1980). Astrophys. J. **242**, 1.

Tifft, W. G. (1972). Astrophys. J. **175**, 613.

Tifft, W. G. (1973). Astrophys. J. **179**, 29.

Tifft, W. G. (1979). Astrophys. J. **233**, 799.

Tifft, W. G., and Gregory, S. A. (1973). Astrophys. J. **181**, 15.

Tifft, W. G., and Gregory, S. A. (1976). Astrophys. J. **205**, 696.

Tifft, W. G., and Gregory, S. A. (1979). Astrophys. J. **231**, 23.

Tifft, W. G., and Tarenghi, M. (1975). Astrophys. J. **199**, 10.

Tifft, W. G., and Tarenghi, M. (1977). Astrophys. J. **217**, 944.

Ulrich, M. H. (1976). Astrophys. J. **206**, 364.

Valtonen, M. J., and Byrd, G. G. (1979). Astrophys. J. **230**, 655.

White, S. D. M. (1976). Mon. Not. R. Astron. Soc. **177**, 717.

Wolf, R. A., and Bahcall, J. N. (1972). Astrophys. J. **176**, 559.

Zwicky, F. (1957). *Morphological Astronomy* (Springer-Verlag, Berlin).

Zwicky, F., and Herzog, E. (1963). *Catalog of Galaxies and of Clusters of Galaxies* (California Institute of Technology, Pasadena), Vol. 2.

Zwicky, F., and Herzog, E. (1966). *Catalog of Galaxies and of Clusters of Galaxies* (California Institute of Technology, Pasadena), Vol. 3.